Climate System Response to External Forcings and Climate Change Projections in CCSM4

GERALD A. MEEHL AND WARREN M. WASHINGTON

National Center for Atmospheric Research, Boulder, Colorado*

JULIE M. ARBLASTER

National Center for Atmospheric Research, Boulder, Colorado, and CAWCR, Bureau of Meteorology, Melbourne, Victoria, Australia*

AIXUE HU AND HAIYAN TENG

National Center for Atmospheric Research, Boulder, Colorado*

CLAUDIA TEBALDI

Climate Central, Princeton, New Jersey

BENJAMIN N. SANDERSON, JEAN-FRANCOIS LAMARQUE, ANDREW CONLEY, WARREN G. STRAND, AND JAMES B. WHITE III

National Center for Atmospheric Research, Boulder, Colorado*

(Manuscript received 30 April 2011, in final form 16 November 2011)

ABSTRACT

Results are presented from experiments performed with the Community Climate System Model, version 4 (CCSM4) for the Coupled Model Intercomparison Project phase 5 (CMIP5). These include multiple ensemble members of twentieth-century climate with anthropogenic and natural forcings as well as single-forcing runs, sensitivity experiments with sulfate aerosol forcing, twenty-first-century representative concentration pathway (RCP) mitigation scenarios, and extensions for those scenarios beyond 2100–2300. Equilibrium climate sensitivity of CCSM4 is 3.20°C, and the transient climate response is 1.73°C. Global surface temperatures averaged for the last 20 years of the twenty-first century compared to the 1986–2005 reference period for six-member ensembles from CCSM4 are +0.85°, +1.64°, +2.09°, and +3.53°C for RCP2.6, RCP4.5, RCP6.0, and RCP8.5, respectively. The ocean meridional overturning circulation (MOC) in the Atlantic, which weakens during the twentieth century in the model, nearly recovers to early twentieth-century values in RCP2.6, partially recovers in RCP4.5 and RCP6, and does not recover by 2100 in RCP8.5. Heat wave intensity is projected to increase almost everywhere in CCSM4 in a future warmer climate, with the magnitude of the increase proportional to the forcing. Precipitation intensity is also projected to increase, with dry days increasing in most subtropical areas. For future climate, there is almost no summer sea ice left in the Arctic in the high RCP8.5 scenario by 2100, but in the low RCP2.6 scenario there is substantial sea ice remaining in summer at the end of the century.

1. Introduction

The Coupled Model Intercomparison Project phase 5 (CMIP5) set of experiments (Taylor et al. 2009, 2012) includes simulations of twentieth-century climate, twenty-first-century climate with four different representative concentration pathway (RCP) scenarios, and,

* The National Center for Atmospheric Research is sponsored by the National Science Foundation.

Corresponding author address: G. Meehl, National Center for Atmospheric Research, P.O. Box 3000, Boulder, CO 80307.
E-mail: meehl@ucar.edu

DOI: 10.1175/JCLI-D-11-00240.1

since climate change does not end in 2100 but is ongoing, extensions of the climate change projections from 2100 to 2300. This paper describes results from the Community Climate System Model, version 4 (CCSM4) for these sets of experiments. In particular, the focus will be on the climate system response to various external forcings, both natural (volcanoes and solar) and anthropogenic [greenhouse gases (GHGs), ozone, land use, sulfate aerosols and carbon (both primary organic and black)] aerosols. Where appropriate, comparisons will be made to previous versions of the model, particularly CCSM3, to show where and how the CCSM4 simulations differ from CCSM3. Results from the climate change projections from CCSM4 shown in the present paper, but with a regional focus over North America, are given by Peacock (2012). Projections of future sea level rise in CCSM4 are given in Meehl et al. (2012).

The purpose of this paper, and why it is included in a CCSM4 Special Collection and not as a regular *Journal of Climate* paper, is to provide a basic overview and description of the CCSM4 simulation characteristics. Thus, it is not a typical *Journal of Climate* paper with analyses that lead to insight into processes and mechanisms. The CCSM4 Special Collection papers are intended to provide the background and description that can then be used as a starting point for more cutting-edge science result papers.

Section 2 includes a brief description of the model and the experiments. Section 3 describes results from the twentieth-century experiments including runs made with the model with single forcings one by one and a sulfate aerosol sensitivity experiment. In section 4 the climate change projections from the twenty-first-century RCP scenario experiments are presented, along with the extensions from 2100 to 2300. Possible future changes in heat and precipitation extremes in CCSM4 are shown in section 5, while some aspects of changes of sea ice are described in section 6. Conclusions will follow in section 7.

2. Model and experiments

The Community Climate System Model, version 4 includes a finite volume nominal 1° (0.9° × 1.25°) 26 level version of the Community Atmosphere Model, version 4 (CAM4) with improved components of ocean, land, and sea ice compared to CCSM3 (Gent et al. 2011). The ocean is a version of the Parallel Ocean Program (POP) with a nominal latitude–longitude resolution of 1° (down to ¼° in latitude in the equatorial tropics) and 60 levels in the vertical. Specifically, grid points in the ocean have a uniform 1.11° spacing in the zonal direction and 0.27° near the equator, extending to 0.54° poleward of 35°N and S. No flux adjustments are used in CCSM4.

TABLE 1. List of experiments and ensemble members for PCM (left column), CCSM3 (middle column), and CCSM4 (right column).

	PCM (T42; 1890–1999)	CCSM3 (T85; 1870–1999)	CCSM4 (FV 1°; 1850–2005)
All forcings	4	5	6
Anthropogenic	4	5	5
Natural	4	5	5
Volcanic	4	2	3
Solar	4	2	3
GHG	4	2	3
Aerosol	—	—	3
Ozone	4	2	3
Black carbon	—	6	3
Sulfate	4	2	3
Sulfate 1.5×			1
Sulfate 2×			1
Land cover	—	—	3
RCP2.6	—	—	6
RCP4.5	—	—	6
RCP6.0	—	—	6
RCP8.5	—	—	6

Experiments analyzed here include twentieth-century simulations (1850–2005) with a combination of anthropogenic and natural forcings (Gent et al. 2011), as well as experiments run with single forcings or a subset of combinations of forcings. The anthropogenic forcings in CCSM4 include time-evolving GHGs, as well as prescribed time- and space-evolving concentrations of tropospheric ozone, stratospheric ozone, the direct effect of sulfate aerosols (there are no indirect effects from sulfate or any other aerosols in CCSM4), and black and primary organic carbon aerosols (Lamarque et al. 2010, 2011). Time-evolving land use and land cover change is also included (Lawrence et al. 2012). A list of model experiments and ensemble members for CCSM4 (as well as earlier models PCM and CCSM3 for comparison) is given in Table 1.

Three-dimensional distributions of ozone (tropospheric and stratospheric) and aerosols were computed offline using the Community Atmospheric Model, version 3.5 modified to run with interactive chemistry (CAM-Chem) and included in the CCSM4 as specified decadal-average monthly concentrations (Lamarque et al. 2011). Note that, while available, the contributions from secondary-organic aerosols are not considered owing to their large uncertainties. For the historical simulations (Lamarque et al. 2010), these concentrations are formed by forcing CAM-Chem with the gridded historical emissions developed by Lamarque et al. (2010), based on a variety of observed inventories of short-lived species, along with zonally averaged distributions of historical greenhouse gases and zonally varying monthly sea surface

temperatures and sea ice concentrations from a CCSM3 historical simulation. Ozone forcing for the future simulations is derived in a similar manner using CAM-Chem forced by RCP emissions of zonally averaged greenhouse gases and zonally averaged sea surface temperatures and sea ice distributions from the CCSM3 Special Report on Emissions Scenarios (SRES) simulation closest to the RCP total radiative forcing at 2100. See Lamarque et al. (2011) for details. Note that all RCPs have a similar evolution of ozone-depleting substances, with chlorofluorocarbons (CFCs) based mostly on the SRES A1 scenario (see Eyring et al. 2010 for details). Stratospheric ozone concentrations do not include effects from the 11-year solar cycle. Note that the ozone forcing used in the CCSM4 simulations is distinct from that of the Atmospheric Chemistry and Climate/Stratospheric Processes and their Role in Climate (AC&C/SPARC) ozone database that has been provided to CMIP5 groups for use in models without interactive chemistry. This was to ensure internal consistency with other aspects of CCSM4. Natural forcings include volcanic aerosols (Ammann et al. 2003) and solar variability (Lean 2000; Wang et al. 2005). The latter is added as an anomaly to the 1850 control value of 1360.9 W m^{-2} (Gent et al. 2011).

Experiments are run for an ensemble of six twentieth-century simulations with a combination of all anthropogenic and natural forcings. Gent et al. (2011) describe the model spinup procedure. In short, the components are developed on their own and then coupled to achieve near-zero top-of-atmosphere radiative balance through several hundred years of integration. Then a preindustrial control run is integrated several hundred years until the system, mostly including the upper ocean, comes into equilibrium. The control run branches at this point for the first twentieth-century integration with subsequent branch points for other twentieth-century simulations separated by a few decades at initial states with different values of meridional overturning circulation (MOC) in the Atlantic that span the range of variability of the MOC (Gent et al. 2011). Single-forcing simulations and combinations of single forcings are also run, and these include 1) five-member ensembles of anthropogenic forcings only and natural forcings only and 2) single-forcing three-member ensembles of volcanic, solar, GHG, ozone, aerosol, black, and organic carbon aerosols only, sulfate aerosols, and land use/land cover change only (see Table 1).

The future climate forcings begin on 1 January 2006 (though the CCSM4 simulations begin in 2005 to provide overlap with the historical and future forcings for a smooth transition in 2006) and follow four mitigation scenarios termed representative concentration pathways (RCPs) (Moss et al. 2010). These scenarios are meant to represent classes of mitigation scenarios that produce emission pathways following various assumed policy decisions that would influence the time evolution of the future emissions of GHGs, aerosols, ozone, and land use/land cover change (Moss et al. 2010).

The emissions of CO_2 for the four RCPs (RCP2.6, RCP4.5, RCP6, and RCP8.5) are shown in Fig. 1a, and the corresponding CO_2 concentrations are in Fig. 1b. The numbering convention in the RCPs represents approximate radiative forcing values for the year 2100 in watts per square meter, though the actual radiative forcing values will depend on the model. Three of the four RCPs (except RCP8.5) have falling emissions of CO_2 by the year 2100 (Fig. 1a). Only RCP2.6 has decreasing CO_2 concentrations by the end of the century (Fig. 1b). The rate of increase of CO_2 concentrations in RCP4.5 is starting to level out by 2100, while RCP6 and RCP8.5 have CO_2 concentrations that are still increasing by 2100 (Fig. 1b). To achieve the decrease of CO_2 concentrations for RCP2.6 in Fig. 1b, it should be noted in Fig. 1a that CO_2 emissions must become negative by about 2070. That is, more CO_2 must be removed from the atmosphere than is being put in, thereby achieving a decreasing trend in CO_2 concentrations by the end of the century.

One way to achieve this in terms of energy usage is, by 2070, to have 20% fossil fuel without carbon capture and storage (CCS), about 45% fossil fuel with CCS, and 35% renewables (some of that includes biomass and CCS as well) and nuclear. In contrast, by 2070 RCP8.5 implies 80% fossil fuels without CCS, no fossil fuel with CCS, and 20% renewables and nuclear (van Vuuren et al. 2011).

With regards to other constituents, the time evolution of GHGs, ozone, aerosols, and land use/land cover are all specified in the respective RCPs (Lamarque et al. 2011). As noted above, ozone and aerosol forcing for the future simulations is derived using CAM-Chem forced by RCP emissions of zonally averaged greenhouse gases and zonally varying monthly sea surface temperatures and sea ice distributions from the CCSM3 SRES simulation closest to the RCP total radiative forcing at 2100. See Lamarque et al. (2011) for details. Volcanic aerosols are held constant at year 2005 values.

The RCP scenarios are all extended from 2100 to 2300, and the corresponding CO_2 concentrations are shown in Fig. 1c. RCP4.5 and RCP6 stabilize by the early 2100s, while RCP8.5 does not level out until the mid-2200s. Meanwhile, RCP2.6 undergoes an ongoing slow decrease of CO_2 concentrations until there is virtually no time rate of change by the end of the twenty-third century. For other constituents, like aerosols and ozone, concentrations are held constant at year 2100 values. There

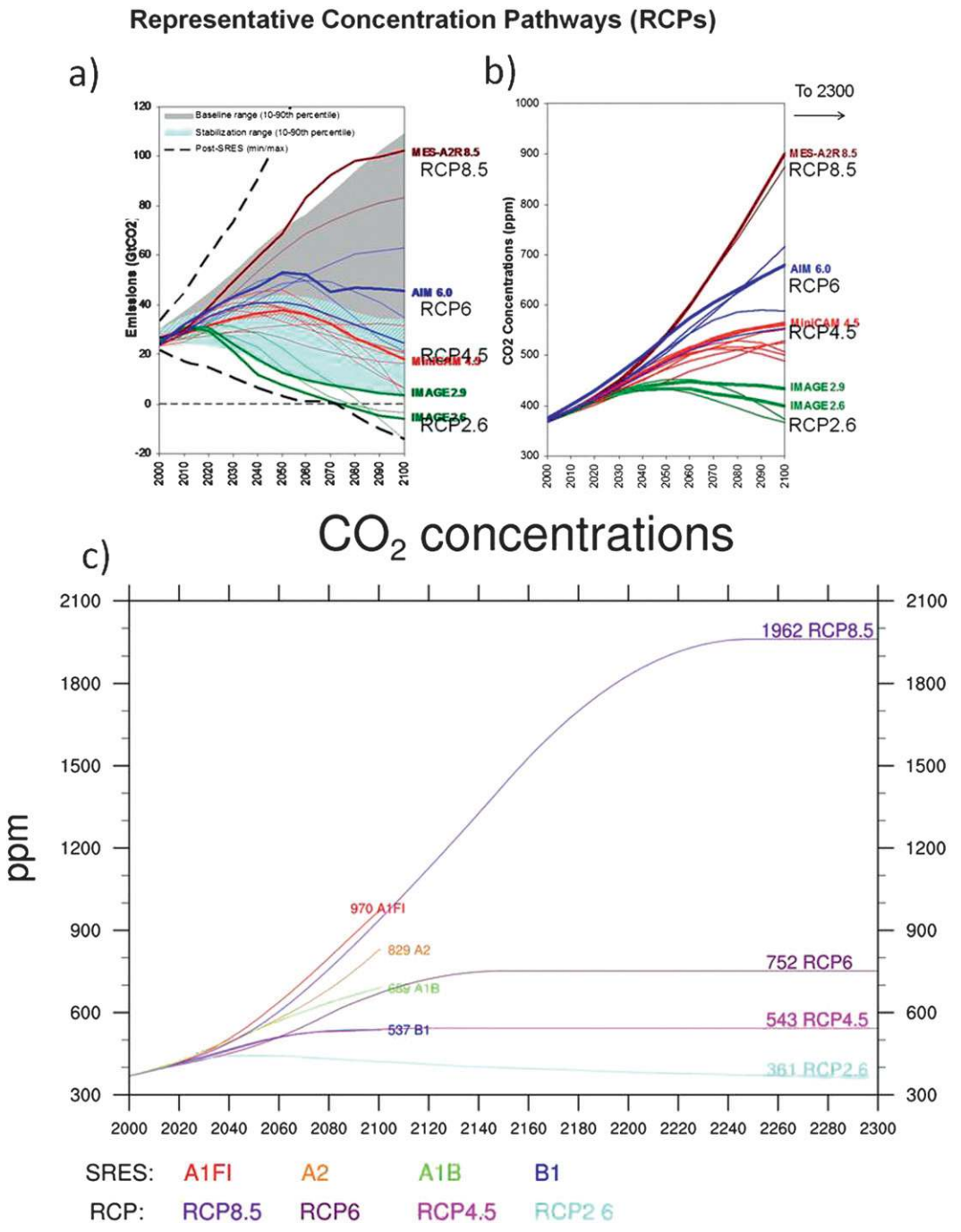

FIG. 1. (a) Carbon dioxide emissions for a number of mitigation scenarios and (b) CO_2 concentrations derived from the emissions in (a), with the four RCPs labeled at the right (after Moss et al. 2010); (c) CO_2 concentrations for the four RCP scenarios to 2100 [from (b)], and extensions to 2300, and CO_2 concentrations from four of the SRES scenarios used in CMIP3; note that CO_2 concentrations are very similar between SRES B1 and RCP4.5 and are nearly comparable for SRES A1FI and RCP8.5. The numbers preceding the scenario labels are the CO_2 concentrations (ppm) at 2100 and 2300.

is a repeating climatological 11-year solar cycle in all the RCP simulations, with the total solar irradiance (TSI) from 2009 to 2140 created by repeating the last four cycles (cycle 20–23), with values from 1965 to 2008 inclusive mapping to 2009–52, 2053–96, 2097–2140. The last 44 values (2097–2140) are replicated six times for the 2141–2404 period, to match what was done for 2009–2140 (three repeats of cycles 20–23). That is, the last 396 values (2009 to 2404) are nine repeats of the last 44 values.

Figure 1c also includes a comparison of CO_2 concentrations in the RCPs with the earlier SRES scenarios (to 2100) used in CMIP3 and described for the CCSM3 by Meehl et al. (2006). SRES B1 is very close to RCP4.5, while RCP8.5 roughly tracks SRES A1FI and is clearly higher than SRES A2. The CO_2 concentrations in RCP6 end up close to those in SRES A1B by 2100, though the time evolution is quite different, with CO_2 increasing much more rapidly in the mid-twenty-first century in A1B than in RCP6. Recall that the extensions that were run from 2100 to 2300 using SRES A1B and B1 were done by holding concentrations of all constituents constant at their year 2100 values. In contrast, Fig. 1c shows that the RCP extensions have some time-evolving changes of CO_2 concentrations beyond 2100.

Results from the standard CCSM3 (e.g., Collins et al. 2006) will be compared, where appropriate, to the new CCSM4 (Gent et al. 2011) in section 3. The CCSM3 had a T85 spectral atmospheric model with 26 levels in the vertical and was coupled to land and sea ice components as well as a nominal one-degree-resolution ocean model going down to about ¼° in the equatorial tropics. Characteristics of the response of CCSM3 to external forcings for twentieth- and twenty-first-century climates were described by Meehl et al. (2006). A subsequent model, Community Earth System Model, version 1 (CESM1)/CAM5, has been developed and descriptions of its simulations will be the subject of an upcoming *Journal of Climate* Special Collection.

General metrics of model response include the equilibrium climate sensitivity and the transient climate response. The equilibrium climate sensitivity comes from an experiment with an active atmospheric component coupled to a nondynamic slab ocean, where the CO_2 concentration doubles instantaneously and the model runs to equilibrium. The equilibrium climate sensitivity is the difference in the globally averaged surface air temperature between the initial control run and the doubled-CO_2 equilibrium. The value is 3.20°C in CCSM4, while in CCSM3 it was quoted by Meehl et al. (2006) to be 2.7°C, and for an earlier model, the Parallel Climate Model (PCM, see Washington et al. 2000), it was 2.1°C. Note that this value for CCSM3 is 2.86°C computed with the most recent version of the slab ocean model (with a major improvement to the way sea ice is handled in the model) coupled to CAM3 (for full description and discussion of processes and metrics see Bitz et al. 2012), indicating a dependence on slab ocean model formulation for the exact value of equilibrium climate sensitivity computed in this way. Also note that the radiative forcing for a doubling of CO_2 (with stratospheric adjustment) is the same in CCSM3 and CCSM4, with a value of 3.5 W m^{-2} [Kay et al. (2012), CCSM4; J. T. Kiehl and C. Shields 2012, personal communication, for CCSM3 using the Hansen method to derive this value, shown to be very similar to that value with stratospheric adjustment].

The transient climate response (TCR) comes from an experiment with a fully coupled model, branching from a control run, and increasing CO_2 at 1% per year compounded. The transient climate response is the difference with the control of the 20-yr globally averaged surface air temperature centered on the time when CO_2 doubles, at roughly 70 years. The value is 1.73°C for CCSM4, 1.5°C for CCSM3, and 1.3°C for PCM. The latter two values are those given by Meehl et al. (2006). Typical values of TCR from calibration studies with models of intermediate complexity include mean values of 1.6°C (5%–95% limits of 1.11°C to 2.34°C, Knutti and Tomassini 2008) and 1.9°C (Stott and Forest 2007). For AOGCMs in the Intergovernmental Panel on Climate Change (IPCC) Fourth Assessment Report (AR4), the 10%–90% confidence limits are about 1°–3°C, with a mean TCR from the CMIP3 AOGCMs of 1.8°C (Meehl et al. 2007). Thus, the CCSM4 TCR value of 1.73°C is close to those other estimates. For further discussion of equilibrium climate sensitivity, transient climate response, and associated processes in CCSM4, see Bitz et al. (2012).

Thus the CCSM4 is somewhat more sensitive to increased CO_2 than the previous model versions. Current estimates of equilibrium climate sensitivity, obtained from multiple lines of modeling, observational, and paleoclimate evidence, range from 2.0° to 4.5°C, with a most likely value of about 3°C (Meehl et al. 2007). Both CCSM3 and CCSM4 fall within the estimated range and are near the most likely value, suggestive that the models are capturing the key first-order processes correctly. This is mostly fortuitous since climate sensitivity is not a tuned parameter and is only determined at the end of the model development process. However, later in this paper the consequences of the magnitude of the forcings in combination with the climate sensitivity will be explored when the time evolution of the model-produced twentieth-century temperature is compared to observations. Observed global surface temperatures are from the HadCRUT3 product (Brohan et al. 2006).

Observed upper-ocean heat content is from Levitus et al. (2009). Monthly sea ice concentrations for the

period 1979–2010 were obtained from the National Snow and Ice Data Center. These data are derived from the *Nimbus-7* Scanning Multichannel Microwave Radiometer and Defense Meteorological Satellite Program *F8*, *F11*, and *F13* Special Sensor Microwave Imager radiances using the NASA team algorithm (Cavalieri et al. 1999).

3. Climate system response to changes in external forcings in twentieth-century simulations

Globally averaged surface air temperature time series for the all-forcings run compared to the natural forcings only and observations are shown in Fig. 2. As for earlier model versions (e.g., Meehl et al. 2004, for PCM), both the all-forcings and natural forcings only show qualitative agreement with the observations up to midcentury with globally averaged surface temperatures increasing from 1900 to 1940 by 0.37° ± 0.13°C in observations (error bars are 95% confidence intervals), 0.20° ± 0.12°C for natural forcings only, and 0.40° ± 0.10°C for all forcings. All level off from about the 1940s to the 1970s. The addition of anthropogenic forcings to the natural forcings produces markedly better agreement with the time evolution of observed temperatures in the latter part of the twentieth century. From 1975 to 2005 the observed warming is 0.40° ± 0.12°C, while in CCSM4 all forcings it is 0.73° ± 0.14°C and there is little net warming over that time period in the natural forcings-only simulations.

The time evolution of global temperature in models and observations has been attributed to having a significant contribution from natural factors in the early part of the century (the increase in solar forcing and relative dearth of volcanic eruptions and their associated cooling), a rough balance between the warming from increasing GHGs and cooling from aerosols in the postwar years until the 1970s, and then the decrease of cooling from aerosols with ever-increasing warming from GHGs after the mid-1970s (e.g., Meehl et al. 2004; Hegerl et al. 2007).

Besides surface air temperature, another relevant metric of the climate system response to external forcings is upper-ocean heat content. Figure 3 shows time series of temperatures averaged over the upper 300 m of ocean for eight different ocean regions plotted from 1957 to 2009. It compares the average of five twentieth-century ensemble members of all CCSM4 forcings, and ensemble mean values from the RCP4.5 simulations for 2006-09, with observations available from Levitus et al. (2009). Until the mid-1990s, at least one of the model ensemble members is close to the observations for each of the ocean regions. After that time, the model simulations

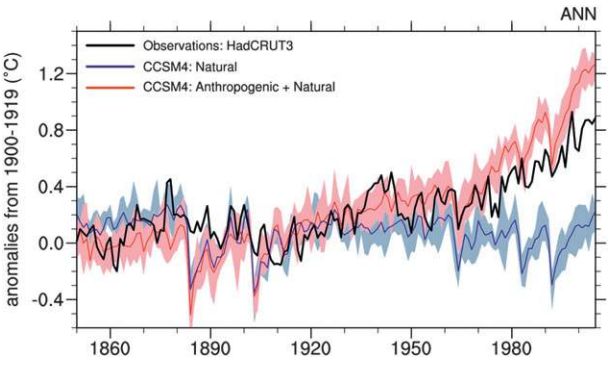

FIG. 2. Time series of annual mean globally averaged surface air temperature (°C) from 1850 through 2005 (anomalies computed relative to 1900–1919) for natural forcings only (five members with volcanoes and solar in blue, shading indicates range of ensemble members) and for natural forcings plus anthropogenic forcings (six members with GHGs, sulfate aerosols, black carbon aerosols, and ozone in red, shading indicates range of ensemble members), and observations from Met Office Hadley Centre–University of East Anglia Climatic Research Unit temperature time series since 1850 (HadCRUT3).

have mostly higher values than the observations in the three southern ocean regions, and lower values in the North Atlantic, possibly related to MOC changes. Though there are caveats that accompany such observed quantities, the model shows relative agreement in most of the global oceans with the observations that have increasing upper-ocean heat content since at least the midtwentieth century. However, the somewhat higher values of globally averaged surface air temperature at the end of the twentieth century in the model compared to observations (Fig. 2) are reflected in the global upper-ocean temperatures (Fig. 3, top left) with similar higher values in that time period that are reflected most strongly in the three southern ocean areas, at the bottom of Fig. 3, as noted above.

Though the equilibrium climate sensitivity of 3.20°C for the CCSM4 is considered to be close to the best estimate of what that number may actually be, as pointed out earlier, the actual response of the model in comparison to observations is a complicated combination of the interaction of the various forcings as well as the climate sensitivity and TCR. To illustrate this for the PCM, CCSM3, and CCSM4 Fig. 4a shows the time series of globally averaged surface air temperature anomalies from the late 1800s to 2000 for PCM and CCSM3 and through 2005 for CCSM4 and the observations (the models are the all-forcings experiments). Overall, the PCM tracks the observations most closely, particularly after the mid-1970s, while CCSM3 is somewhat warmer, and CCSM4 is warmer still, compared to observations in the latter part of the century (as noted above). The models react with greater global cooling than observed

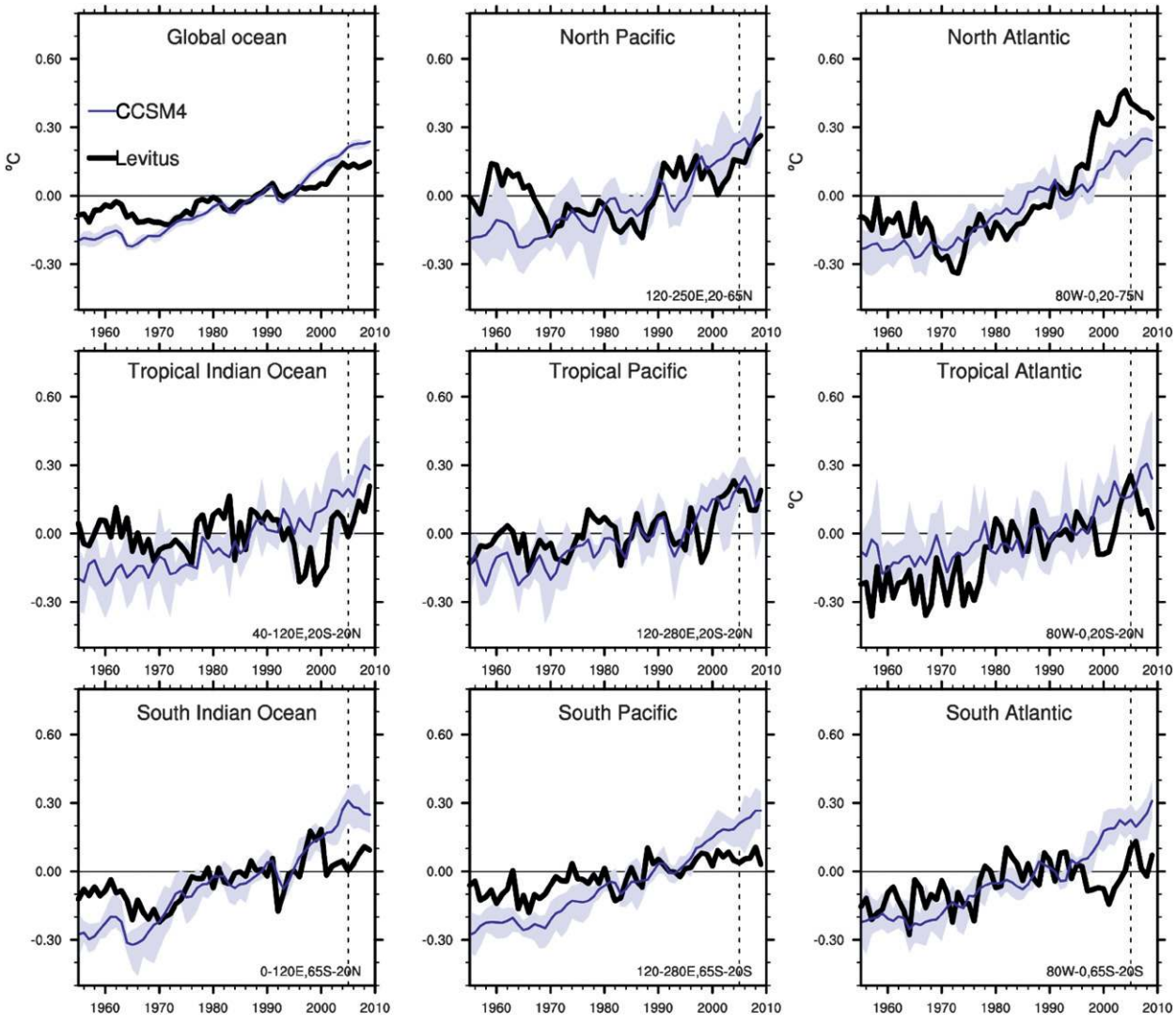

FIG. 3. Upper-ocean heat content (upper 300 m) anomalies (°C) relative to 1980–99 for CCSM4 (ensemble average is solid blue line, range is shaded), and observations in black (Levitus et al. 2009) for various ocean areas as indicated in each panel, with the boundaries for each area at bottom right in each panel. The vertical dashed lines denote the year 2005, and values for 2006-09 for CCSM4 are the RCP4.5 simulations.

to volcanic eruptions (e.g., cooling after El Chichón in 1982 and Mt. Pinatubo in 1991) though the occurrence of El Niño events in 1982–83 and 1991–92 complicate a completely direct comparison between models and observations. This is because the model simulations are single realizations of interannual ENSO variability [see Deser et al. (2012) for a more complete description of ENSO in CCSM4], and our main objective here is to compare trends and the model response to external forcings. Nevertheless, the models have different magnitudes of the forcings that would affect the global temperature, including the radiative forcing from the direct effect of sulfate aerosols of -0.56 W m^{-2} for PCM (Forster et al. 2007), about -0.8 W m^{-2} for CCSM3 (W. Collins 2012, personal communication), and -0.45 W m^{-2} for CCSM4 (these values will be discussed in more detail below with regards to Fig. 7). Therefore, the difference in response has a contribution from the differences in equilibrium climate sensitivity and transient climate response in the models. Consequently, it could be expected that the CCSM4, with the largest sensitivity and lowest negative radiative forcing from the direct effect of sulfate aerosols, would be warmest by the late twenty-first century.

Since the CCSM4 all-forcings experiments are warmer than observed with a warming from 1975 to 1999 of 0.44° ± 0.15°C (compared to 0.43°C for PCM, 0.49°C for CCSM3, and 0.40°C ± 0.15°C for observations), it may

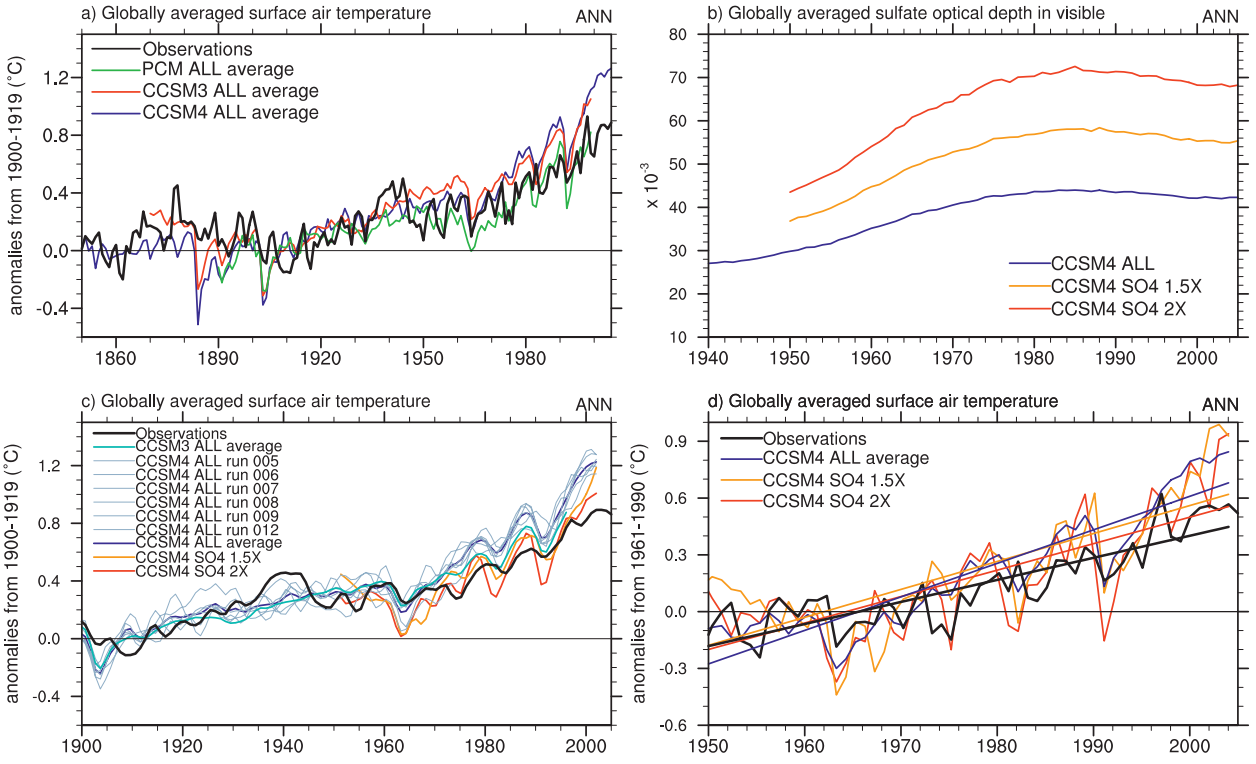

FIG. 4. (a) Time series of annual-mean globally averaged surface air temperature (°C) from 1850 through 2005 (anomalies computed relative to 1900–19) for the ensemble average of CCSM4 simulations (blue, as shown in Fig. 2), 1870–1999 for the ensemble average of CCSM3 simulations (red), and 1890–1999 for the ensemble average of PCM simulations (green), and observations (black) as in Fig. 2; (b) time series of sulfate direct effect optical depth from CCSM4 standard run (bottom line), increased by 1.5 (middle line), and (top) increased by 2.0 (top line); (c) time series of 5-yr running mean annually averaged global surface air temperatures for the six individual ensemble members of CCSM4, the ensemble average for CCSM4, and the 1.5 and 2.0 sulfate aerosol increase experiments, as well as the HadCRUT3 observations (see color key in figure); and (d) annual-mean globally averaged surface air temperatures and the linear trends from 1950 to 2005 for the experiments.

be tempting to speculate that, if the negative radiative forcing from the indirect effect of sulfate aerosols were included, the CCSM4 could be cooled down somewhat and come into closer agreement with the observations. Neither the PCM nor CCSM3 had the indirect of sulfate aerosols either, but their lower-equilibrium climate sensitivities and TCR likely contributed to their better agreement with the observations. Presumably, if enough negative forcing from the missing sulfate aerosol indirect effect were added to CCSM4, it could be made to be in closer agreement with the observations.

To explore the sensitivity of the projected temperature response to uncertainties in the forcing, two sensitivity experiments are performed. Since the total sulfate aerosol forcing has been estimated to be roughly -1.1 ± 0.4 W m^{-2} (Murphy et al. 2009), in the first experiment we multiply the time-evolving sulfate aerosol concentration anomalies after 1950 by 1.5 to produce a forcing of roughly -0.68 W m^{-2} and in the second we multiply by 2.0 after 1950 (Fig. 4b), resulting in a forcing of about -0.90 W m^{-2}. Both of these forcings are below the best estimate of -1.1 W m^{-2} from Murphy et al. and thus represent conservative values for the sulfate forcing. The way this is implemented in the model is that the sulfate concentration at year N (12 monthly values) is computed by taking the original year N values minus year 1850 values and, where the difference is greater than 0, multiply by 1.5 or 2.0 for each of the two experiments, then add those back to the year N values. The conditional on 0 is to avoid negative sulfate values. The sensitivity experiments are branched from one of the all-forcings ensemble members.

Results for the 5-yr running means of globally averaged surface air temperatures are shown in Fig. 4c. Indeed, by increasing the negative forcing from sulfate aerosols in the two experiments, both are somewhat cooler than most of the ensemble members of the standard CCSM4. The observed global warming from 1950 to 2005 is 0.65° ± 0.10°C, the ensemble average 1950–2005 temperature trend for CCSM4 all forcings is 0.99° ± 0.12°C, and by increasing the sulfate aerosol concentrations by 50% and 100%, the temperature increase for

that same time period is 0.82° ± 0.19°C and 0.78° ± 0.19°C, respectively (Figs. 4c,d). Thus, it could be argued that increasing the sulfate aerosol direct effect was successful in better simulating the late century observed temperature trend. However, inspection of the actual time evolution of the temperatures in Fig. 4c shows that the response to volcanic eruptions, with already overly strong cooling in the standard CCSM4, becomes even stronger with the increase of negative radiative forcing from sulfate aerosols in the lower troposphere (sulfate aerosols in the stratosphere from volcanic eruptions are kept at their standard values in the two sensitivity experiments; the reason for this response is an interesting science question that is beyond the scope of this paper but is currently being investigated). Thus, the juxtaposition of greater negative forcing in the lower troposphere with the volcanic aerosols in the stratosphere actually produces worse agreement with the observations. It can be seen from this exercise that it is quite difficult to accurately reproduce the time-evolving response to external forcings in the climate system by simply increasing radiative forcing of one component. This is due to unforeseen interactions of different processes that respond to the forcings in different ways in the model. Trying to include factors to mimic the effect of missing processes can produce undesirable side effects. Thus, climate modeling is less about trying to reproduce the time evolution of twentieth-century climate with an arbitrary set of parameters and more about understanding and representing the underlying physical processes that drive observed behavior in the climate system.

To further illustrate the climate system response to forcings during the twentieth century, the anthropogenic-only results are shown for globally averaged surface air temperature in Fig. 5a for CCSM3 compared to CCSM4 and the observations. Both models show cooler-than-observed conditions in the late 1800s but then track the observations reasonably well until CCSM4 becomes somewhat warmer than observed in the latter part of the twentieth century. The natural-only experiments are shown similarly in Fig. 5b, with greater agreement in temperature response between the two models. With just the GHGs (Fig. 5c), there is less agreement between the models and observations, particularly for CCSM4 in the late 1800s (a somewhat different representation of GHGs was used in CCSM4 compared to CCSM3, thus contributing to the differences between the two models during that time), with more of a gradual warming trend through the entire time period and warmer than observed temperatures in late century comparable to the CCSM3. This suggests that the differences seen in the late twentieth century are at least partly associated with non-GHG anthropogenic forcings.

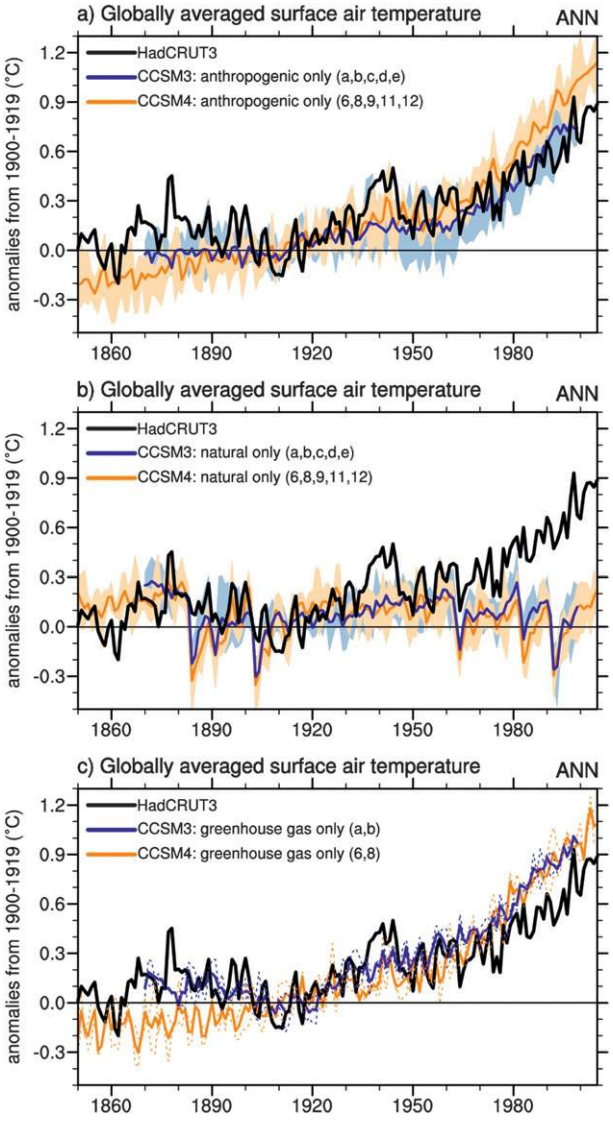

FIG. 5. (a) Time series of annual-mean globally averaged surface air temperature (°C) from 1850 through 2005 (anomalies computed relative to 1900–1919) for the ensemble average (solid line) and range (shading) for CCSM3 anthropogenic forcings only (blue, five members) and CCSM4 anthropogenic forcings only (orange, five members) compared to observations as in Fig. 2; (b) as in (a) but for natural forcings only experiments from the CCSM3 and CCSM4; and (c) as in (a) but for greenhouse gas only experiments from the CCSM3 and CCSM4 (two members only for each, as denoted by dotted lines).

For CCSM4, the natural forcings contribute to the warming in the early part of the century until the 1950s, the anthropogenic-only experiments perform best compared to observations from the late 1940s onward, and GHG-only are too cool early and too warm later on with a more gradual warming trend throughout. Thus, CCSM3

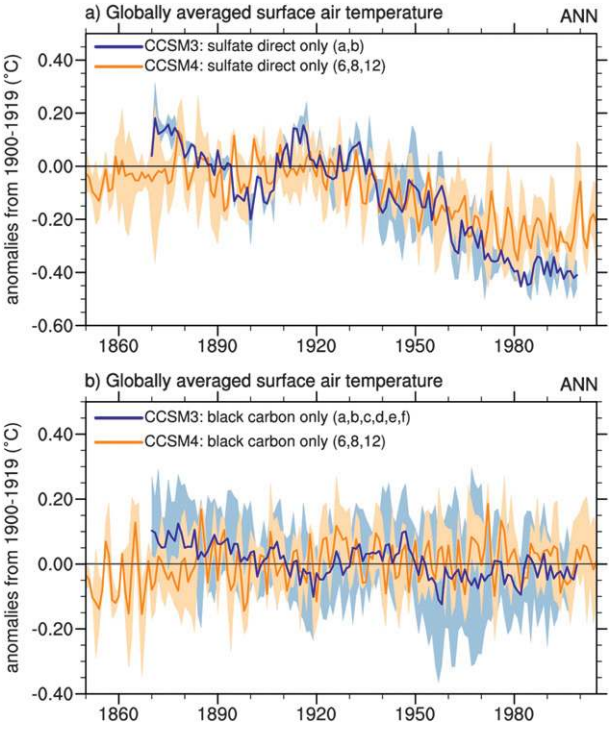

FIG. 6. (a) As in Fig. 5 but for sulfate aerosol direct effect only experiments with two members from CCSM3 (solid blue line ensemble average, blue shading range of ensemble members) and three members from CCSM4 (solid orange line ensemble average, orange shading range of ensemble members); (b) as in Fig. 5 but for black carbon aerosols only, six members from CCSM3 (blue line and shading) and three members from CCSM4 (orange line and shading).

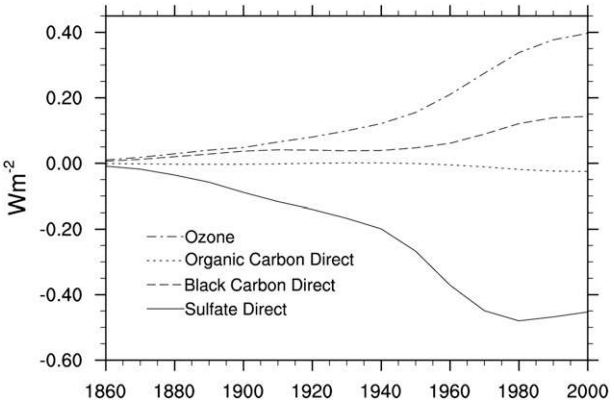

FIG. 7. Time series of radiative forcing in CCSM4 at top of troposphere for ozone (dash–dot line), organic carbon direct effect (dotted line), black carbon direct effect (dashed line), and sulfate aerosol direct effect (solid line).

and CCSM4 have significant structural differences, and this contributes to their different abilities to reproduce the general aspects of globally averaged climate change, particularly in the latter part of the twentieth century as seen in Fig. 5a.

To examine further the response to aerosols of CCSM3 and CCSM4, Fig. 6a shows the globally averaged surface air temperature time series for the sulfate-only experiments. The radiative forcing for the sulfate direct effect is different as noted above (-0.80 W m^{-2} for CCSM3, -0.56 W m^{-2} for PCM, and -0.45 W m^{-2} for CCSM4 in Fig. 7). Additional time series of radiative forcing for several other constituents in CCSM4 are also shown in Fig. 7. Radiative forcing at year 2000 for black carbon is $+0.14$ W m^{-2}, organic carbon is -0.03 W m^{-2}, and tropospheric ozone is $+0.40$ W m^{-2}. The net radiative forcing from these non-GHG forcings is $+0.06$ W m^{-2}.

Returning to Fig. 6a where the effects of sulfate aerosols are isolated, as could be expected from the different radiative forcing noted above, CCSM3 cools more by the end of the twentieth century (roughly -0.40°C) compared to CCSM4 (around -0.25°C). Looking at the linear trends (K decade^{-1}) from 1950 to 1999, PCM is -0.19, CCSM3 is -0.33, and CCSM4 is -0.13. Therefore CCSM4 with the least negative radiative forcing has the smallest cooling trend, CCSM3 has the biggest negative radiative forcing and the greatest cooling, with PCM in between for both radiative forcing and cooling. The sulfate aerosol loading in CCSM4 is less than in CCSM3 by about 12% (Fig. 8, globally averaged sulfate aerosol optical depth for 1999 of 0.047 in CCSM3 and 0.042 in CCSM4).

There are a number of factors in the models that relate to the response to sulfate aerosols. In CCSM3 there was a sulfur cycle model that took SO_2 emissions and converted those to SO_4 aerosol concentrations that were internally consistent with the meteorology of the model. There is no sulfur cycle model in CCSM4, but offline concentrations of SO_4 were calculated and included in the atmospheric chemistry model (Lamarque et al. 2010). These may not always be consistent with the meteorology of the CCSM4 twentieth-century simulations.

With regards to the carbon (black and organic) aerosols, these concentrations were put into CCSM3 in a simplistic way by scaling an estimated global distribution of present-day black carbon aerosols back in time based on population (Meehl et al. 2006). The black carbon aerosols in CCSM4 were generated in a more realistic fashion offline (Lamarque et al. 2010, 2011) with time-evolving distributions of concentrations based on emissions. Following Collins et al. (2002), the effects of moisture on the aerosol optical properties were not included in CCSM4. This factor, combined with a lower burden than CCSM3, contributes to reduced carbon optical depths in CCSM4 (globally averaged optical depth of 0.004) compared to CCSM3 (globally averaged

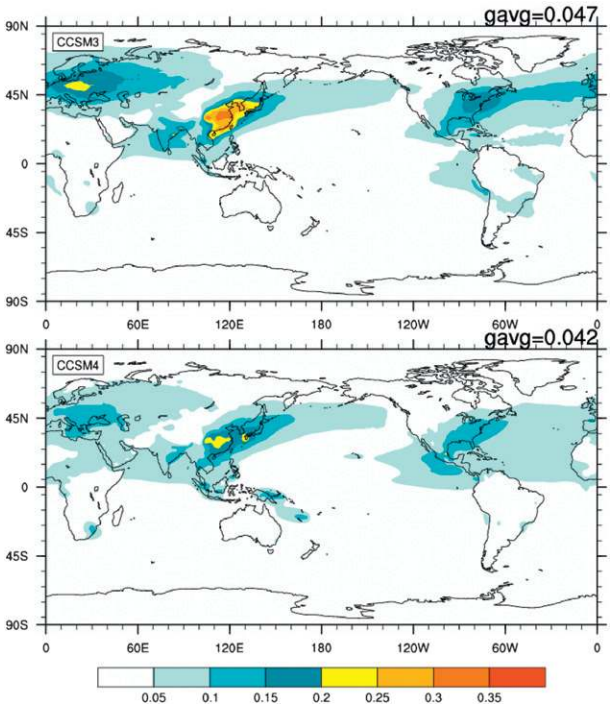

FIG. 8. Sulfate aerosol optical depth for 1999 from (a) CCSM3 and (b) CCSM4: global average optical depths are given at top right of each panel.

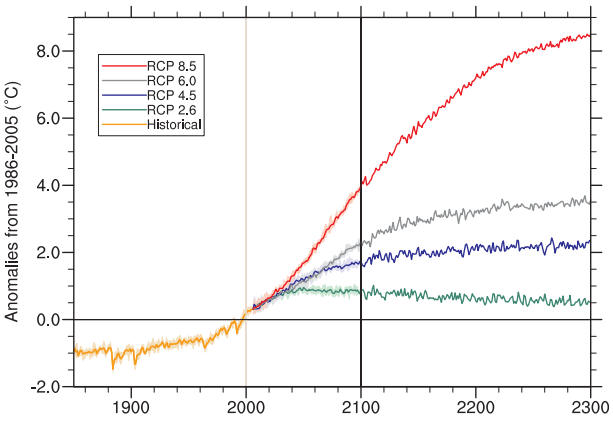

FIG. 9. Time series of annual globally averaged surface air temperature anomalies (relative to 1986–2005 base period (°C) from 1865 to 2300 for CCSM4. Solid colored lines indicate ensemble average ± one std dev of the ensemble members (six prior to 2006, six from 2006 to 2100, and one each for the extensions beyond 2100). The year 2100 is denoted by vertical solid line, and there is lack of shading for standard deviations after 2100 since there is only one ensemble member for each scenario.

optical depth of 0.023). However, there is no indication of a strong negative bias in the atmospheric carbon concentrations or deposition in CCSM4 when compared to other model studies [see Lamarque et al. (2010, 2011) for more details]. The result is a slightly positive globally averaged temperature response to black carbon aerosols in CCSM4 compared to slightly negative in CCSM3 in Fig. 6b, though the considerable overlap in the range of ensemble members makes these slight differences nearly indistinguishable from a near-zero net temperature response. Though the globally averaged temperature response is small, regional forcing due to black and organic carbon can produce significant regional changes in climate, such as over the south Asian monsoon (e.g., Meehl et al. 2008) with teleconnections to North America (Teng et al. 2012).

4. Climate change projections for the twenty-first century

Figure 9 shows the time series of globally averaged surface air temperature for six members of the twentieth-century all-forcings simulations, six members of the twenty-first-century RCP mitigation scenario simulations, and single-member extensions to 2300 for the four RCP scenarios. The ensemble average warming for the last 20 years of the twenty-first century minus the period 1986–2005 is +0.85°C for RCP2.6, +1.64°C for RCP4.5, +2.09°C for RCP6, and +3.53°C for RCP8.5.

Beyond the twenty-first century, RCP6 and RCP8.5 continue to warm with the ongoing increases of CO_2 (Fig. 1), so by the end of the twenty-third century the globally averaged surface air temperature difference for 2281–2300 (for those single members) minus the 1986–2005 average (for the historical ensemble members that correspond to the single ensemble member extensions) is +3.56° and +8.40°C, respectively. For RCP4.5, CO_2 concentrations effectively stabilize after 2100 (Fig. 1), but owing to climate change commitment (e.g., Meehl et al. 2005), the climate system continues to warm somewhat such that the globally averaged surface air temperature difference for 2281–2300 (for that single member) minus 1986–2005 (for the historical ensemble member that corresponds to that single ensemble member extension) is +2.21°C. However, for RCP2.6, CO_2 concentrations slowly decrease after 2100 (Fig. 1) so that the climate begins to cool a bit. The globally averaged surface air temperature difference for 2281–2300 (for that single member) minus 1986–2005 (for the historical ensemble member that corresponds to that single ensemble member extension) for RCP2.6 is +0.52°C. This value is lower than the ensemble average warming of +0.85°C for RCP2.6 given above for the last 20 years of the twenty-first century minus the period 1986–2005.

Thus, the globally averaged surface air temperature changes post-twenty-first century (2281–2300 minus 2081–2100 calculated for those single ensemble members) are −0.31°C for RCP2.6, +0.59°C for RCP4.5

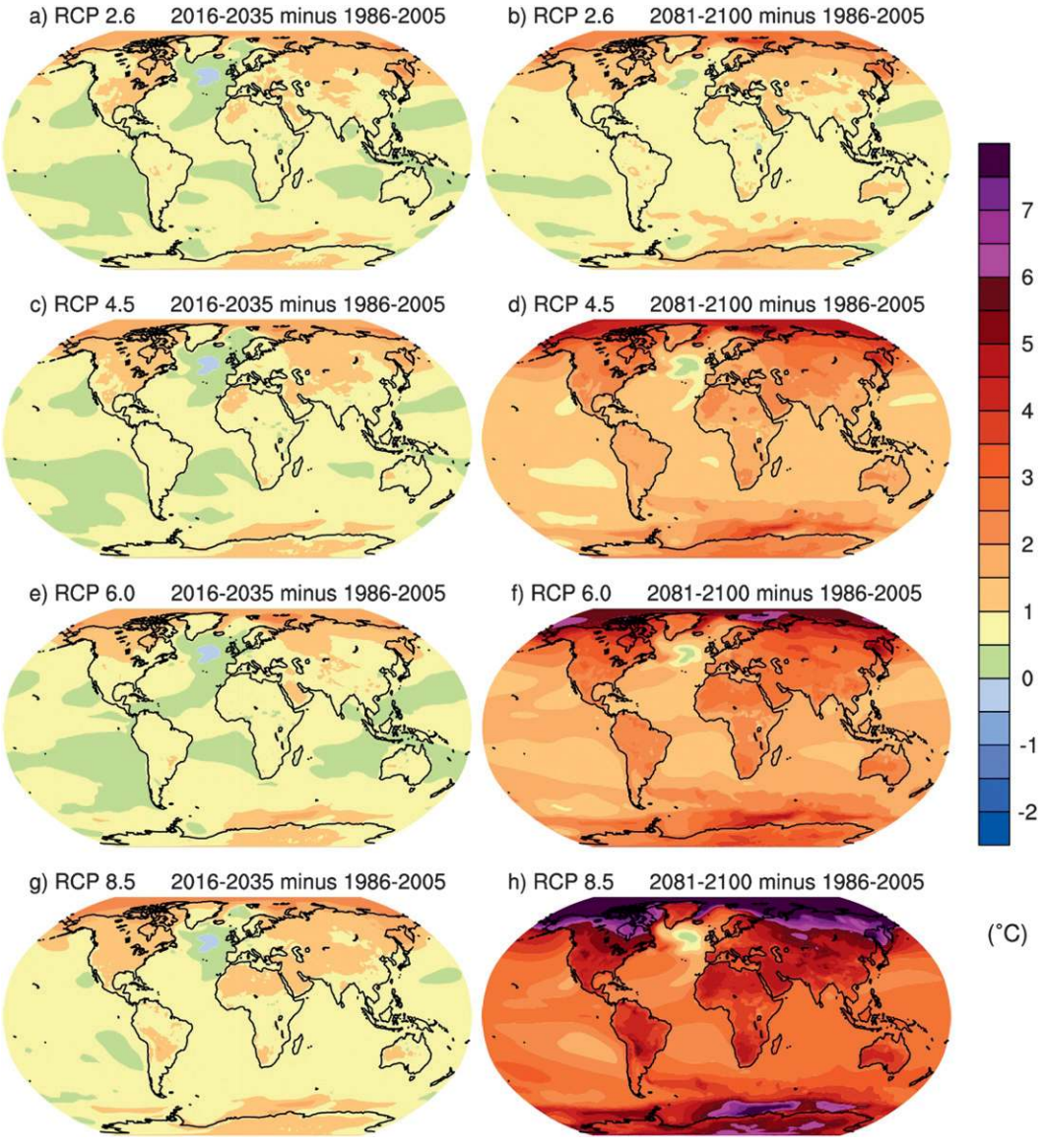

FIG. 10. Surface air temperature differences (°C), all calculated in relation to a 1986–2005 base period for (a),(b) RCP2.6; (c),(d) RCP4.5; (e),(f) RCP6.0; and (g),(h) RCP8.5 for two time periods: (left) one near-term (2016–35) and (right) one longer term for the end of the twenty-first century (2081–2100).

(a measure of climate change commitment), and +1.42° and +4.81°C for RCP6 and RCP8.5, respectively.

Of particular interest is whether any of the RCP mitigation scenarios achieves the target of avoiding 2°C warming above preindustrial, widely claimed to be the threshold of dangerous climate change (e.g., Meinshausen et al. 2009). Only RCP2.6 reaches this goal, with warming averaged from 2081–2100 minus 1850–1900 of +1.83°C. However, as noted earlier in Fig. 1, to achieve this target requires negative emissions of CO_2 starting by about 2070.

Geographical distributions of surface temperature difference patterns are shown in Fig. 10 for an early century time period (2016–35) and for late twenty-first century (2081–2100), and for the four RCP scenarios. As in previous model versions, land areas warm faster than oceans, and the lower emission scenarios warm less than the higher emission scenarios. Northern Hemisphere high-latitude regions show greatest warming, and the North Atlantic warms less than almost anywhere else. The magnitude of warming is similar across scenarios for near-term climate change (left column of Fig. 10), but choice of scenario makes a much bigger difference for the amount of climate change in the late twenty-first century (right column of Fig. 10). Looking beyond 2100,

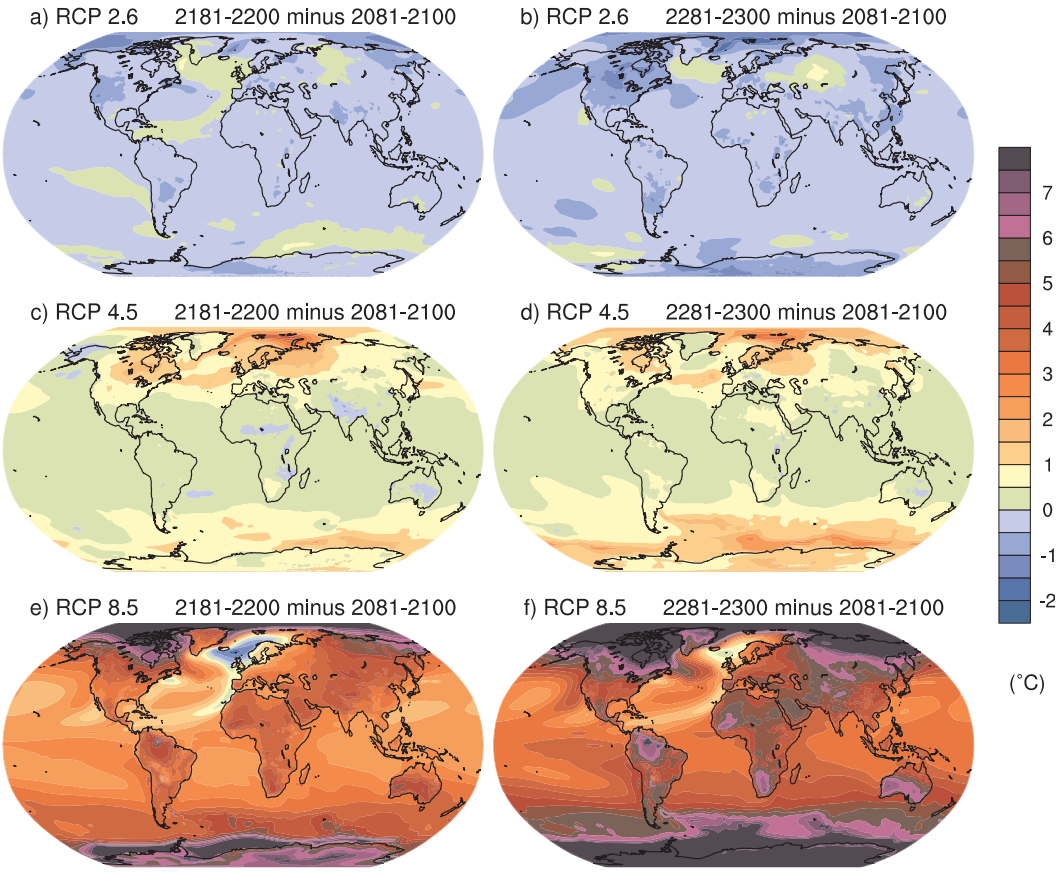

FIG. 11. Surface air temperature differences (°C), all calculated in relation to a base period at the end of the twenty-first century (2081–2100) for (top) RCP2.6, (middle) RCP4.5, and (bottom) RCP8.5 for two time periods: (left) one at the end of the twenty-second century (2181–2200) and (right) one for the end of the twenty-third century (2281–2300).

Fig. 11 shows surface temperature differences for three of the RCP scenarios in Fig. 10 but for the end of the twenty-second century minus the end of the twenty-first century (left column), and the end of the twenty-third century minus end of twenty-first century (right column). Since RCP2.6 is cooling somewhat after CO_2 concentrations begin to decrease in the twenty-first century, there is mostly cooling after 2100 (Figs. 11a,b). However, warming continues with small amplitude in RCP4.5 (Figs. 11c,d), which is a sign of climate change commitment since the GHG concentrations are not increasing during this period, and greater magnitude temperature increase occurs in successive centuries in RCP8.5 where GHGs continue to increase.

Figure 12 shows geographical plots of precipitation differences for the same time periods and for three of the scenarios as in Fig. 10. As in previous model versions, there are increases in precipitation in many tropical regions and decreases in subtropical areas, with comparable changes in precipitation across scenarios for near-term climate, and greater scenario differentiation for longer-term climate change. With regards to sea level pressure (SLP) changes in Fig. 13, there are decreases at high latitudes in each hemisphere, indicating a shift to positive phases of the Northern Annular Mode (NAM) and Southern Annular Mode (SAM) with greater increases of GHGs (Arblaster and Meehl 2006; Arblaster et al. 2011). As the planet warms, higher pressure dominates in the North Pacific, in the North Atlantic, and over the circumpolar Southern Ocean around 45°–60°S, with a corresponding expansion of the Hadley Cell (e.g., Meehl et al. 2007). There are scenario time dependencies for the magnitude of change similar those noted previously for temperature and precipitation.

Sea level pressures are calculated in CCSM4 following the European Centre for Medium-Range Weather Forecasts formulation, as in previous model versions. Extrapolation is based on a fixed environmental lapse rate involving surface and near-surface pressure with some specific adjustments based on surface and mean sea level temperatures. Here we apply an additional correction to the monthly output to overcome erroneous values over high elevations. We follow the method of

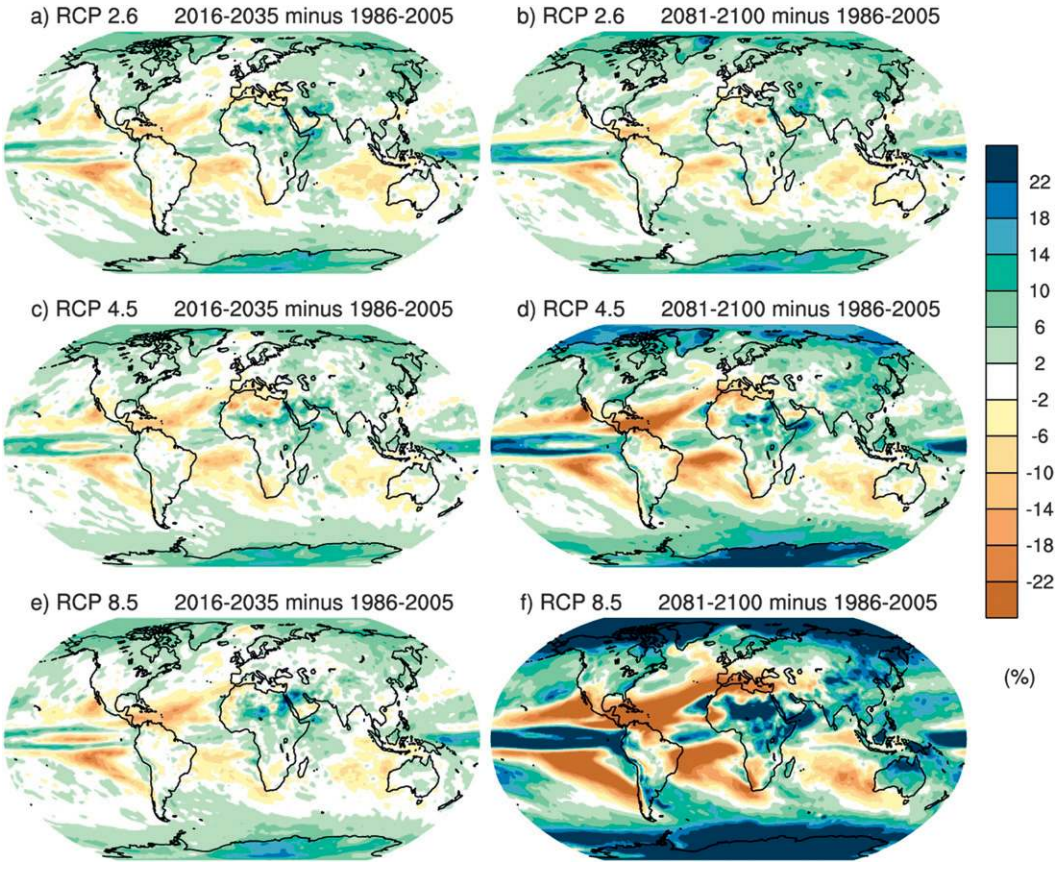

FIG. 12. As in Fig. 11 but for precipitation differences (%) calculated in relation to a 1986–2005 base period for two time periods: (left) one near-term (2016–2035) and (right) one longer term for the end of the twenty-first century (2081–2100).

Trenberth et al. (1993) by replacing SLP for all gridpoints above 2000 m with an interpolation from lower gridpoints to the east and west. Without this correction the SLP changes over Greenland and other high mountain ranges exhibit extremely large increases with increased warming. No correction is available over Antarctica, which thus shows large positive values over much of the continent. This issue was also weakly present in the CCSM3 SLP projections (Meehl et al. 2006) but presumably the higher climate sensitivity of the CCSM4 has led to its amplification in the RCP scenario simulations.

Zonal temperature changes (Fig. 14) for the end of the twenty-first century, shown for the low (RCP2.6) and high (RCP8.5) mitigation scenarios, indicate robust warming throughout the troposphere and cooling in the stratosphere for RCP 8.5 with amplified warming over the lower troposphere in the Northern Hemisphere (NH) high latitudes. The maximum in warming in the tropical upper troposphere is associated with lapse rate feedbacks and results in a steepening of the equator to pole temperature gradient near the tropopause. In RCP2.6 the smaller radiative forcing change results in much weaker warming overall and the dominance of Southern Hemisphere (SH) stratospheric ozone recovery and Arctic amplification in the temperature change pattern. The competing effects of the GHG and ozone forcings on the zonal winds result in an equatorward shift (negative anomalies near 60°S, positive values near 40°S) in the SH extratropical jet for RCP2.6 and a poleward shift (positive anomalies near 60°S, negative values near 40°S) for RCP8.5. In the NH the extratropical jet responds to the decreased meridional temperature gradient at the surface (associated with polar amplification) and increased meridional temperature gradient aloft with a muted response under RCP2.6 and a weak poleward shift under RCP8.5. An increase in the Brewer–Dobson circulation is evident from increased winds in the tropical stratosphere.

The average meridional overturning circulation (MOC), defined as the maximum of the Atlantic meridional overturning streamfunction below 500 m, is 25.0 Sv

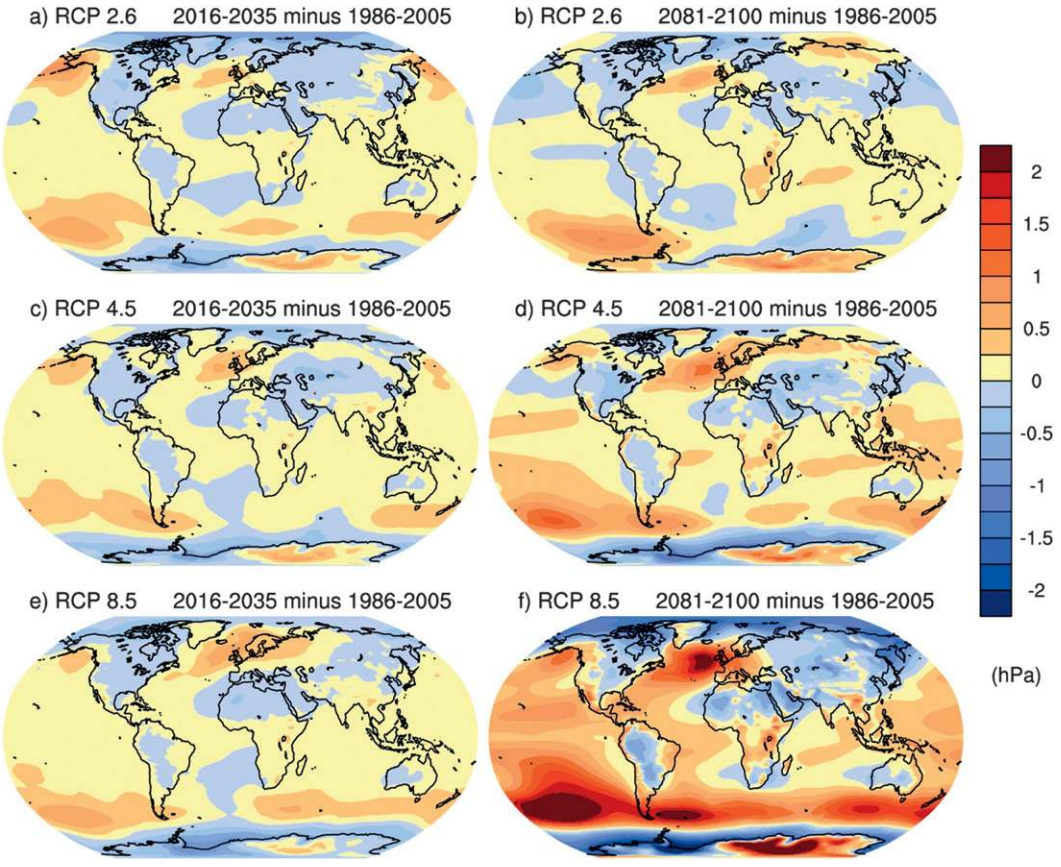

FIG. 13. As in Fig. 12 but for sea level pressure differences (hPa).

(Sv $\equiv 10^6$ m^3 s^{-1}) in the CCSM4 control run, a bit higher than in the CCSM3 control run (21.8 Sv, Bryan et al. 2006). At 25°N the maximum MOC strength is 20.3 Sv in the control run. During the twentieth century, the mean maximum MOC is 24.3 Sv and the MOC strength at 25°N is 19.7 Sv, This value is comparable to estimates of the observed MOC strength that include, for example, from the Rapid Climate Change Programme (RAPID) observations at 26.5°N, a value of 18.7 ± 5.6 Sv (Cunningham et al. 2007); from ship hydrographic measurements at 25°N, values of 22.9 Sv in 1957, 18.7 Sv in 1981, 19.4 Sv in 1992, 16.1 Sv in 1998, and 14.8 Sv in 2004 (Bryden et al. 2005); from inverse modeling at 24°N, 18 ± 2.5 Sv (Lumpkin and Speer 2007); from another inverse modeling calculation for North Atlantic Deep Water (NADW) in the North Atlantic, a value of 15 ± 2 Sv, and NADW at 30°S with a value of 23 ± 3 Sv (Ganachaud and Wunsch 2000); and using the RAPID observations, Kanzow et al. (2007) computed MOC variability of ±5.7 Sv at 26.5°N, agreeing well with the other observations already noted (e.g., Ganachaud and Wunsch 2000; Cunningham et al. 2007; Kanzow et al. 2007; Lumpkin and Speer 2007). With regards to changes in the MOC in the North Atlantic, as the planet warms during the twentieth century the MOC decreases in CCSM4, but then mostly recovers to midtwentieth-century values by the end of the twenty-first century in the RCP2.6 mitigation scenario (Fig. 15). The MOC almost recovers to midtwentieth-century values in RCP4.5 and RCP6, but does not recover by 2300 in RCP8.5. This is another measure of irreversibility, whereby with aggressive mitigation in RCP2.6 there is a significantly different outcome for the MOC compared to much less effective mitigation in RCP8.5.

5. Projected changes in heat and precipitation extremes

As has been noted in previous studies (e.g., Meehl and Tebaldi 2004; Tebaldi et al. 2006), as the average temperatures increase, the heat wave intensity (defined as the average minimum temperature during the warmest three consecutive nights of the year) increases as well almost everywhere, with the increase proportional to the forcing. Thus, in Fig. 16, RCP2.6 shows the smallest

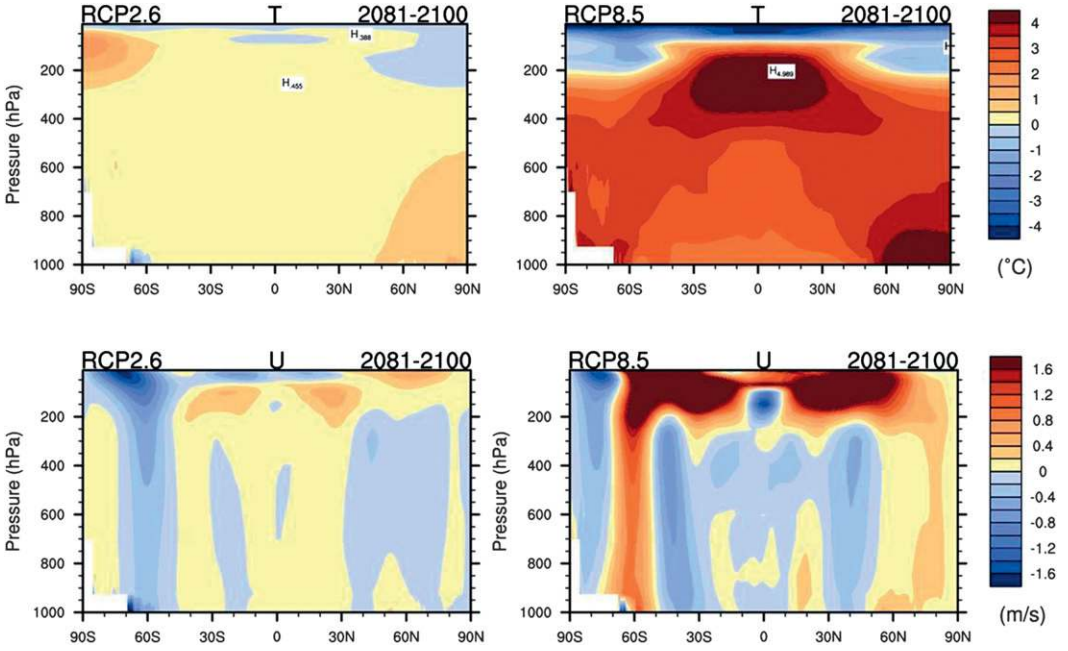

FIG. 14. (top) Zonal mean temperature (°C) and (bottom) zonal wind (m s^{-1}) changes for (left) RCP2.6 and (right) RCP8.5 based on five-member ensemble mean changes: 2081–2100 minus 1986–2005.

amplitude increases in heat wave intensity, with RCP4.5 in the middle and RCP8.5 with the largest increases in heat wave intensity.

Also shown previously (e.g., Tebaldi et al. 2006), since the warmer atmosphere can hold more moisture that provides a source for precipitation, the precipitation intensity [defined as the annual total precipitation divided by the number of wet days, e.g., Tebaldi et al. (2006)] increases in CCSM4 almost everywhere (Fig. 17). However, for changes in annual average precipitation in Fig. 12, it is the combination of precipitation intensity and the changes in dry days (defined as the number of days between precipitation events) that is important. Dry days increase in most subtropical areas in CCSM4 (Fig. 18), again a function of scenario with RCP2.6 showing the smallest changes in dry days, and RCP8.5 the largest. However, there are some interesting patterns that emerge as a consequence of the combination of precipitation intensity and dry days. For example, over areas of California and Nevada, where previous multimodel projections have shown an average decrease in precipitation and the implied greater risk of drought (Meehl et al. 2007), the CCSM4 shows little consistent change in annual average precipitation by the end of the twenty-first century in that region (Fig. 12). This is because, in previous multimodel studies, precipitation intensity increases, but dry days increase even more, thus producing average decreases of precipitation over the southwest United States (Tebaldi et al. 2006). However, in CCSM4, though precipitation intensity increases in that region, there is an average *decrease* in dry days (Fig. 18). That, in combination with increased precipitation intensity, results in little consistent annual-average change in precipitation in those areas of California and Nevada in Fig. 12. This is an example of how average changes in precipitation must be interpreted in terms of how the precipitation occurs with regards to extremes. The reason for these changes is an interesting science question that is beyond the scope of this paper but is currently under investigation.

6. Projected changes in sea ice

In this section, projections of sea ice extent are shown, though more details and explanations are given for the Arctic in Vavrus et al. (2012) and Jahn et al. (2012) and for the Antarctic by Landrum et al. (2012). Figure 19 shows the time series of average ice extent for the Arctic and Antarctic for seasons February–April (FMA) and August–October (ASO), times of the year when the Arctic sea ice is at its seasonal maximum and minimum extent, and vice versa for the Antarctic. For the Arctic there is reasonably good agreement with the observations in terms of the CCSM4 simulation of sea ice extent for the last part of the twentieth century, with both observations and model showing trends for decreases of

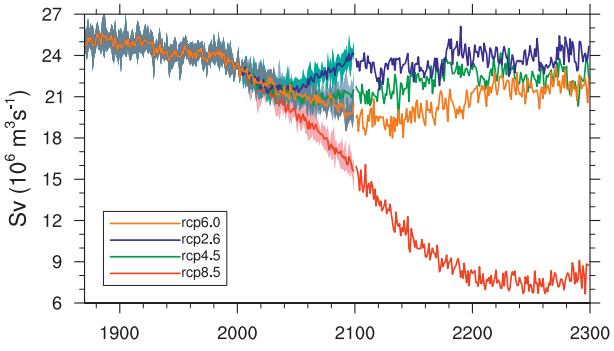

FIG. 15. Index of the MOC in the Atlantic taken as the largest value of meridional overturning streamfunction (Sv) below 500-m depth. Solid lines are ensemble averages for twentieth and twenty-first centuries with shading indicating the range of the ensemble. After 2100, solid lines indicate single members.

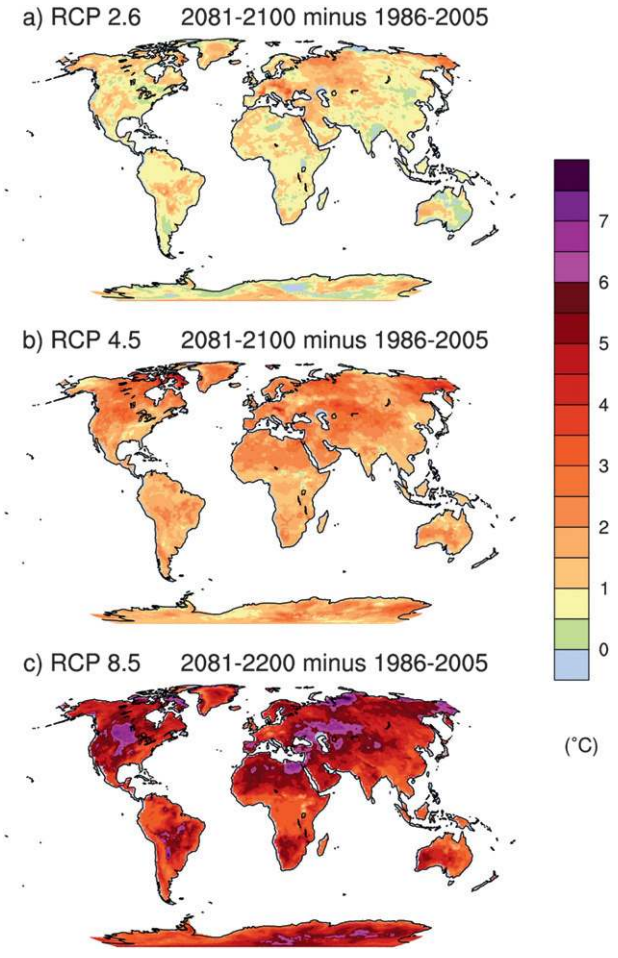

FIG. 16. Changes in average heat wave intensity (°C) between 2081–2100 and 1986–2005. Heat wave intensity is defined as the average minimum temperature during the warmest three consecutive nights of the year. Single ensemble members for three RCPs are compared: (top) RCP 2.6, (middle) 4.5, and (bottom) 8.5. In the Northern Hemisphere the year is defined as 1 Jan through 31 Dec and in the Southern it is defined as 1 Jul through 30 Jun.

sea ice extent, though the Arctic sea ice extent in ASO seems to be decreasing faster in the observations than in the CCSM4. Projected changes in sea ice extent are proportional to the size of the radiative forcing and global temperature increase in the different RCPs. Only RCP8.5 shows a near vanishing of sea ice at the end of the summer season by 2100. Beyond 2100, sea ice extent mostly stabilizes at late twenty-first-century values in RCP4.5 and RCP2.6, except for the ASO season for RCP2.6 where there is a slight increase of Arctic sea ice in the twenty-second and twenty-third centuries. In RCP8.5 there are ongoing decreases of Arctic sea ice in the winter FMA season until, by 2300, there is almost no sea ice left in winter, lagging the disappearance of summer sea ice in that scenario by about two centuries.

For the Antarctic in Fig. 19, the model simulates more ice than observed in both seasons by about a factor of two in FMA and roughly 10% in ASO. This is due in part to excessively strong westerly winds near 50°–60°S that drive a large equatorward meridional ice transport and overly extensive sea ice (Landrum et al. 2012). Contrary to recent observations, the model shows a decreasing sea ice area at the end of the twentieth century and ongoing decreases of sea ice in the future, with biggest losses in RCP8.5 in FMA. The Antarctic sea ice extent is stabilized in RCP2.6 in both seasons after 2100, but continues to slowly decline in RCP4.5 in winter and summer. Antarctic summer sea ice is totally gone in RCP8.5 by about 2200 and stabilizes in winter at a low value by about 2250. Further discussion of these simulations and features is given in Landrum et al. (2012).

Geographical polar projection plots of Arctic sea ice extent for the twenty-first century are shown in Fig. 20. Dashed lines show the present-day extent of sea ice in the Arctic. By 2100, RCP8.5 shows the largest decreases in Arctic sea ice relative to the other RCPs, mainly in the Bering Sea and North Atlantic, though most areas of the Arctic remain ice covered in winter even in RCP8.5, the scenario with the greatest warming. However sea ice loss is much more evident at the end of the summer season in Fig. 21. There is virtually no ice left in RCP8.5 by the end of the twenty-first century, with only some low concentrations in areas immediately north of Greenland and the Canadian archipelago. Meanwhile, for RCP2.6 where CO_2 concentrations are decreasing by the end of the century, much more sea ice remains at the end of the summer, with notable losses only appearing north of Bering Strait. Therefore, with regards to summer Arctic sea ice in the late twenty-first century, it makes a big difference as to which future climate change scenario is followed.

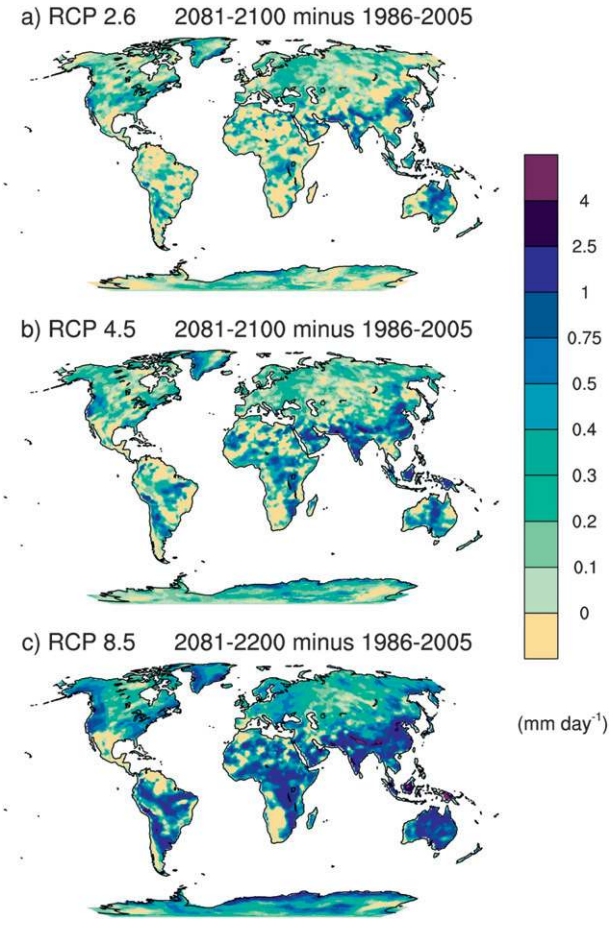

FIG. 17. As in Fig. 16 but for changes in precipitation intensity (mm day^{-1}), defined as the total annual precipitation divided by the number of wet days (days with precipitation greater than or equal to 1 mm day^{-1}), 2081–2100 minus 1986–2005.

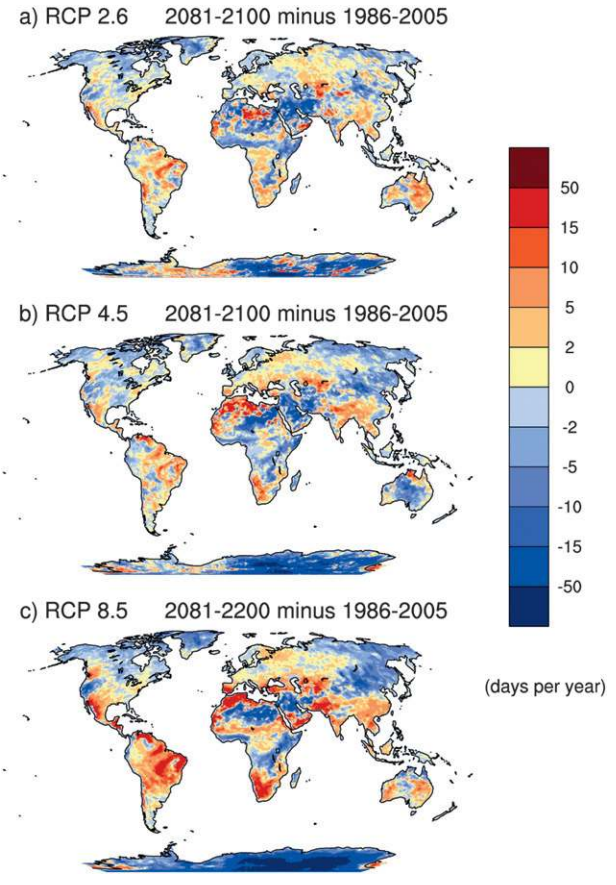

FIG. 18. As in Figs. 16 and 17 but for changes in average length of dry spells (dry days), defined as the length of the longest stretch of consecutive days with precipitation less than 1 mm day^{-1} during the year; year defined as in Fig. 16.

7. Conclusions

The CCSM4 has been run for the CMIP5 experiments, and results are shown here from multiple ensemble members of twentieth-century climate with all-forcings as well as single-forcing runs and experiments with combinations of forcings. Equilibrium climate sensitivity of CCSM4 is 3.20°C, and the transient climate response is 1.73°C (for a full description see Bitz et al. 2012). The value of the former is higher by about 25% compared to CCSM3 (equilibrium climate sensitivity of 2.7°C, though this value has recently been calculated to be about 2.9°C with a new slab ocean formulation) and 50% higher compared to PCM (equilibrium climate sensitivity of 2.1°C). None of these model versions includes the indirect effect of sulfate aerosols. This factor, plus the higher climate sensitivity, likely contributes to a late twentieth-century climate simulation in CCSM4 that is somewhat warmer than the other two models and the observations. Sensitivity experiments are performed with CCSM4 to test the effects of increasing the negative radiative forcing from the direct effect of sulfate aerosols. Though the trend in the late twentieth-century globally averaged temperatures in CCSM4 is reduced by ramping up the sulfate aerosol forcing, thus bringing the model in closer agreement to observations by that measure, the oversensitive response to volcanoes (which is an interesting science problem now being studied) makes the comparison to observations worse in terms of the time evolution of globally averaged temperatures. This highlights the difficulties associated with trying to reproduce the time series of globally averaged surface temperature by simply adjusting the magnitude of the forcing.

Among the single-forcing simulations with CCSM4, there is some agreement with the time evolution of globally averaged surface air temperatures with only GHGs, though differences in the agreement with

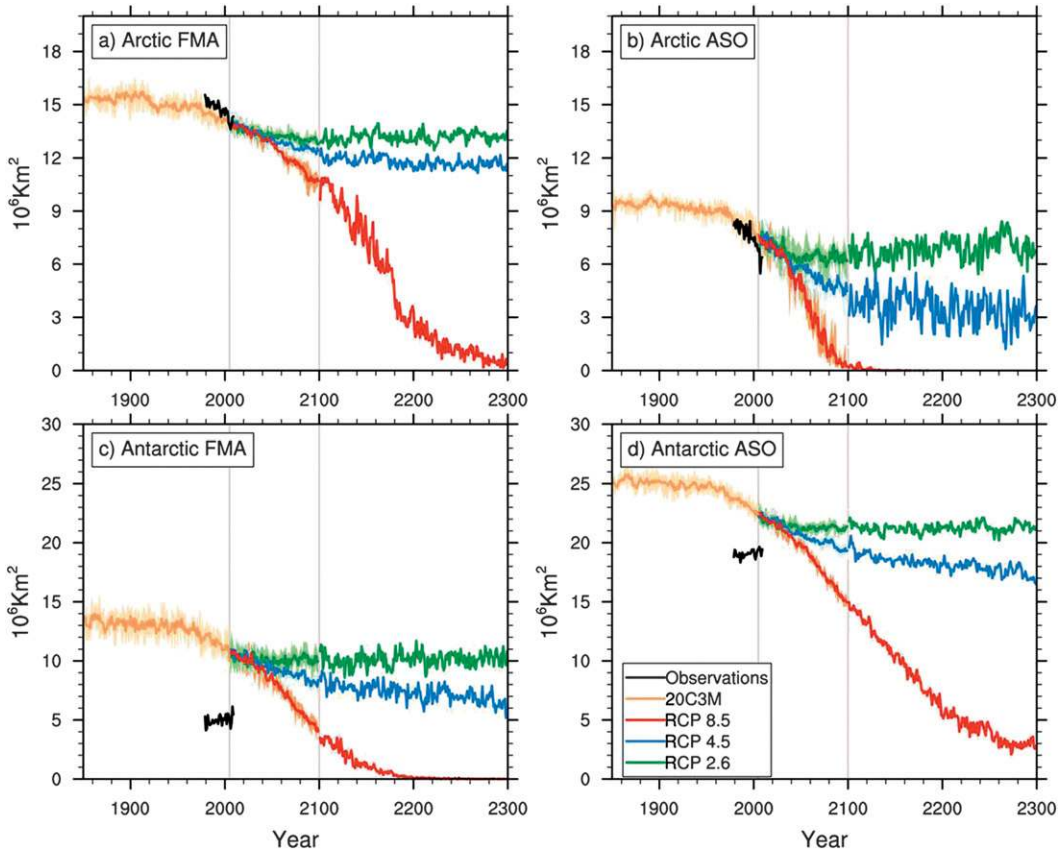

FIG. 19. (a) Arctic sea ice extent (10^6 km^2) for twentieth century (orange), RCP2.6 (green), RCP4.5 (blue), RCP8.5 (red), and observations (black) for the February–April (FMA) season; (b) as in (a) but for the August–October (ASO) season; (c) as in (a) but for the Antarctic sea ice; and (d) as in (b) but for the Antarctic sea ice. Solid lines with shading indicate ensemble average and the range of the ensemble members. There are six ensemble members prior to 2006, six from 2006–2100, and one each for the extensions beyond 2100: seen by lack of shading for standard deviations after 2100 since there is only one ensemble member for RCP2.6, RCP4.5, and RCP8.5.

observations at various times point to the importance of non-GHG forcing, particularly in the late twentieth century. There is a different representation of black carbon aerosols in CCSM4 compared to CCSM3, with a decrease in optical depths in the former compared to the latter partly due to not including moisture effects on the aerosols. However, there is little discernable net global temperature response in either model run with black and organic carbon only.

Results are presented from the twenty-first-century RCP mitigation scenarios (RCP2.6, RCP4.5, RCP6, and RCP8.5) and extensions beyond 2100 to 2300. Globally averaged temperatures at the end of the twenty-first century show that, by following the low mitigation scenario (RCP2.6), warming relative to the preindustrial climate is +1.83°C, which is below the widely cited desired target of 2°C above preindustrial. To achieve this target RCP2.6 specifies negative CO_2 emissions starting around the year 2070. Global surface temperatures averaged for the last 20 years of the century compared to the 1986–2005 reference period for five-member ensembles from CCSM4 are +0.85°, +1.64°, +2.09°, and +3.53°C for RCP2.6, RCP4.5, RCP6.0, and RCP8.5, respectively.

Patterns of future surface temperature change in CCSM4 agree with previous results in that there is greater warming over continents compared to oceans, larger amplitude warming in the Arctic than elsewhere, and less warming overall in the North Atlantic compared to almost anywhere else. Precipitation increases in the warmer climate occur in most areas of the deep tropics and midlatitudes, with decreases in large areas of the subtropics. Sea level pressure changes indicate more positive phases of the NAM and SAM in a future warmer climate, with lower SLP in the Arctic and higher pressure in the subtropical North Pacific and North

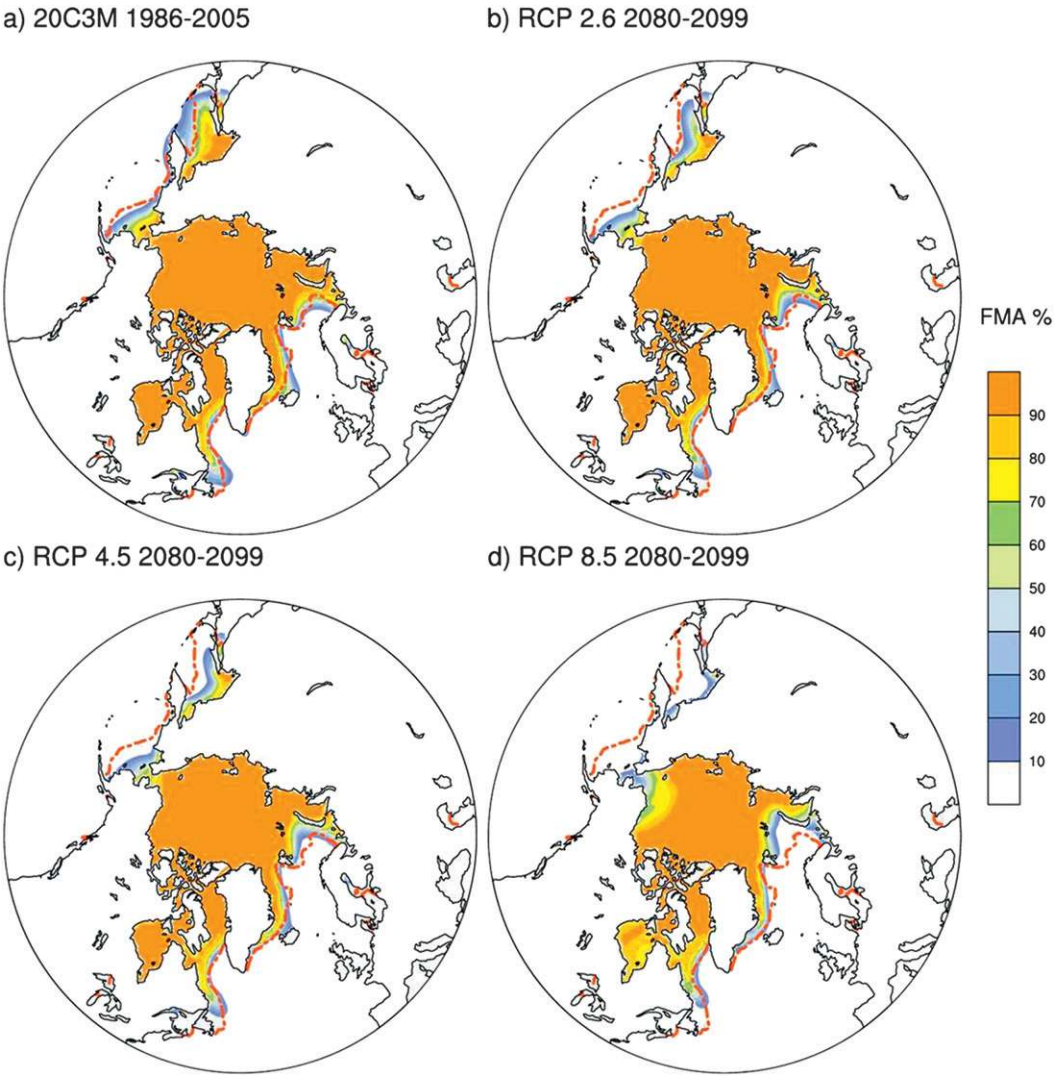

FIG. 20. For February–April Arctic (a) late twentieth-century (1986–2005 average) sea ice concentration (%) and late twenty-first-century (2080–2099 average) sea ice concentration for (b) RCP2.6, (c) RCP4.5, and (d) RCP8.5. Dotted red line is observed sea ice extent for end of twentieth century.

Atlantic. Choice of scenario makes little difference to the magnitude of near-term climate change, but is very important for the amount of long-term climate change.

The MOC in the Atlantic recovers from a weakening trend with the warming over the twentieth century to early twentieth-century values by 2100 in RCP2.6. In RCP4.5 and RCP6 there is partial recovery, and in RCP8.5 there is no recovery of the MOC by 2300.

Heat wave intensity is projected to increase almost everywhere in CCSM4 as the twenty-first century proceeds, with the size of the increase proportional to the forcing. Precipitation intensity is also projected to increase almost everywhere, with the biggest increases of dry days in subtropical regions. However, there is a lack of consistent drying over areas of California and Nevada seen in earlier multimodel ensembles, as evidenced by annual mean precipitation. This is a result of a combination of increases in precipitation intensity and decreases in dry days, as opposed to earlier studies that showed decreases in annual mean precipitation over that region being produced by increases in precipitation intensity and compensated for by increases in dry days.

The simulation of Arctic sea ice concentration in CCSM4 corresponds well to observations except in late summer when observed sea ice concentrations have decreased faster than in the model. The Antarctic

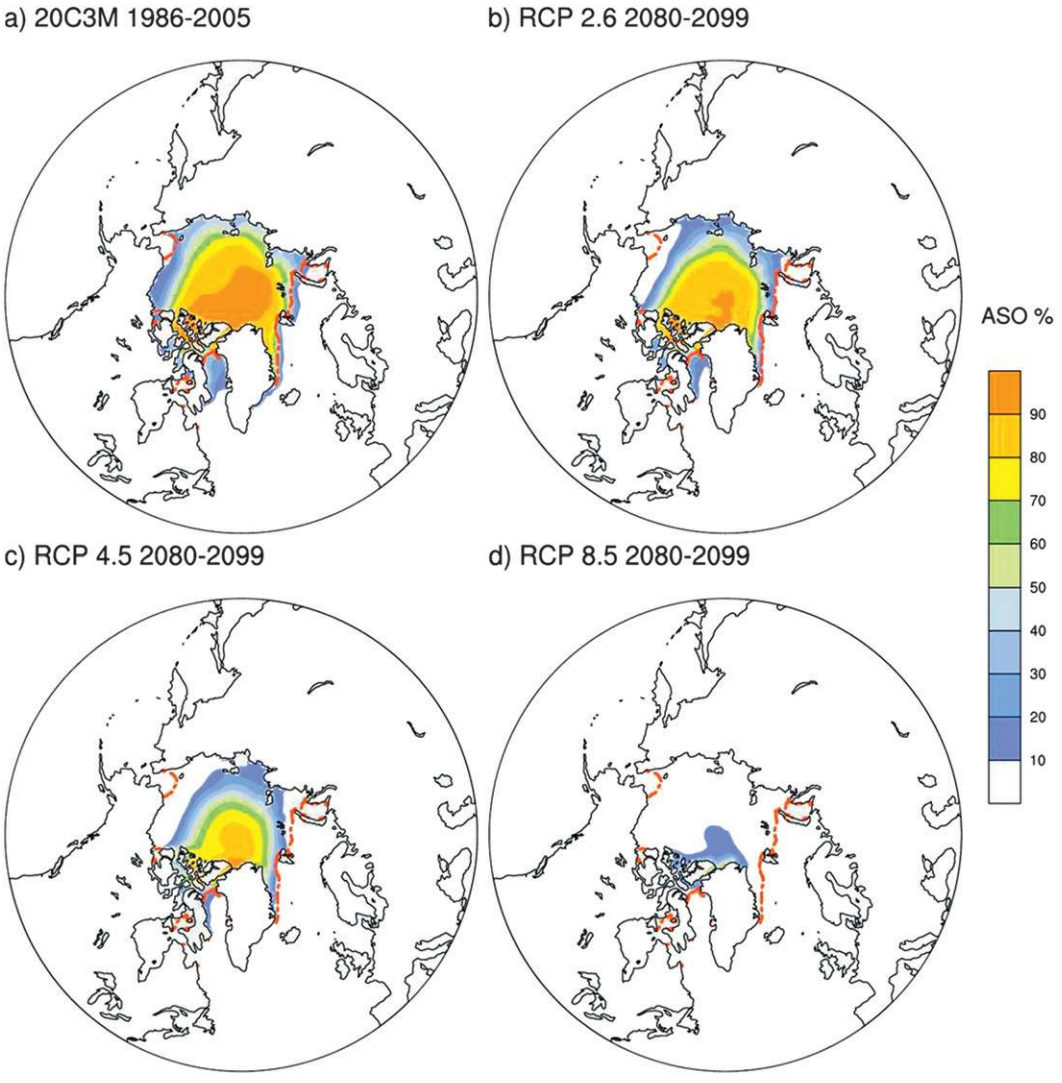

FIG. 21. As in Fig. 20 but for August–October Arctic.

compares less well with observations, with overextensive sea ice year-round and a decreasing trend in sea ice concentration in the latter twentieth century compared to slight increases in observations. For future climate, there is almost no sea ice left at the end of the twenty-first century in summer in the Arctic in the high RCP8.5 scenario, but in the low RCP2.6 scenario there is substantial sea ice at that time of year indicating that, for summer Arctic sea ice, it does make a considerable difference as to which path we choose to follow with regards to future emissions.

Acknowledgments. This research used computing resources of the Climate Simulation Laboratory at the National Center for Atmospheric Research (NCAR), which is sponsored by the National Science Foundation; the Oak Ridge Leadership Computing Facility, which is supported by the Office of Science of the U.S. Department of Energy under Contract DE-AC05-00OR22725; and the National Energy Research Scientific Computing Center, which is supported by the Office of Science of the U.S. Department of Energy under Contract DE-AC02-05CH11231. We acknowledge Adrianne Middleton, Andy Mai, and Diane Feddema at NCAR who helped perform the model runs, as well as members of the Community Earth System Model (CESM) Software Engineering Group who also made important contributions. Portions of this study were supported by the Office of Science, Biological and Environmental Research, U.S. Department of Energy, Cooperative Agreement DE-FC02-97ER62402 and the National Science Foundation.

REFERENCES

Ammann, C. M., G. A. Meehl, W. M. Washington, and C. Zender, 2003: A monthly and latitudinally varying volcanic forcing dataset in simulations of 20th century climate. *Geophys. Res. Lett.,* **30,** 1657, doi:10.1029/2003GL016875.

Arblaster, J. M., and G. A. Meehl, 2006: Contribution of various external forcings to trends in the Southern Annular Mode. *J. Climate,* **19,** 2896–2905.

——, ——, and D. Karoly, 2011: Future climate change in the Southern Hemisphere: The competing effects of ozone and greenhouse gases. *Geophys. Res. Lett.,* **38,** L02701, doi:10.1029/2010GL045384.

Bitz, C. M., K. M. Shell, P. R. Gent, D. Bailey, G. Danabasoglu, K. C. Armour, M. M. Holland, and J. T. Kiehl, 2012: Climate sensitivity in the Community Climate System Model, version 4. *J. Climate,* **25,** 3053–3070.

Brohan, P., J. J. Kennedy, I. Harris, S. F. B. Tett, and P. D. Jones, 2006: Uncertainty estimates in regional and global observed temperature changes: A new dataset from 1850. *J. Geophys. Res.,* **111,** D12106, doi:10.1029/2005JD006548.

Bryan, F. O., and Coauthors, 2006: Response of the North Atlantic thermohaline circulation and ventilation to increasing carbon dioxide in CCSM3. *J. Climate,* **19,** 2382–2397.

Bryden, L. H., H. R. Longworth, and S. A. Cunningham, 2005: Slowing of the Atlantic meridional overturning circulation at 25°N. *Nature,* **438,** 655–657, doi:10.1038/nature04385.

Cavalieri, D. J., C. L. Parkinson, P. Gloersen, J. C. Comiso, and H. J. Zwally, 1999: Deriving long-term time series of sea ice cover from satellite passive-microwave multisensor data sets. *J. Geophys. Res.,* **104** (C7), 15 803–15 814.

Collins, W. D., P. J. Rasch, B. E. Eaton, D. W. Fillmore, J. T. Kiehl, T. C. Beck, and C. S. Zender, 2002: Simulation of aerosol distributions and radiative forcing for INDOEX: Regional climate impacts. *J. Geophys. Res.,* **107,** 8028, doi:10.1029/2000JD000032.

——, and Coauthors, 2006: The Community Climate System Model, version 3 (CCSM3). *J. Climate,* **19,** 2122–2143.

Cunningham, S. A., and Coauthors, 2007: Temporal variability of the Atlantic meridional overturning circulation at 26.5°N. *Science,* **317,** 935–937.

Deser, C., and Coauthors, 2012: ENSO and Pacific decadal variability in Community Climate System Model Version 4. *J. Climate,* **25,** 2622–2651.

Eyring, V., and Coauthors, 2010: Sensitivity of 21st century stratospheric ozone to greenhouse gas scenarios. *Geophys. Res. Lett.,* **37,** L16807, doi:10.1029/2010GL044443.

Forster, P., and Coauthors, 2007: Changes in atmospheric constituents and in radiative forcing. *Climate Change 2007: The Physical Science Basis,* S. Solomon et al., Eds., Cambridge University Press, 129–234.

Ganachaud, A., and C. Wunsch, 2000: Improved estimates of global ocean circulation, heat transport and mixing from hydrographic data. *Nature,* **408,** 453–457.

Gent, P., and Coauthors, 2011: The Community Climate System Model, version 4. *J. Climate,* **24,** 4973–4991.

Hegerl, G. C., and Coauthors, 2007: Understanding and attributing climate change. *Climate Change 2007: The Physical Science Basis,* S. Solomon et al., Eds., Cambridge University Press, 663–745.

Jahn, A., and Coauthors, 2012: Late-twentieth-century simulation of Arctic sea ice and ocean properties in the CCSM4. *J. Climate,* **25,** 1431–1452.

Kanzow, T., and Coauthors, 2007: Observed flow compensation associated with the MOC at 26.5°N in the Atlantic. *Science,* **317,** 937–941.

Kay, J. E., M. M. Holland, C. Bitz, A. Gettelman, E. Blanchard-Wrigglesworth, and A. Conley, and D. Bailey, 2012: The influence of local feedbacks and northward heat transport on the equilibrium Arctic climate response to increased greenhouse gas forcing. *J. Climate,* in press.

Knutti, R., and L. Tomassini, 2008: Constraints on the transient climate response from observed global temperature and ocean heat uptake. *Geophys. Res. Lett.,* **35,** L09701, doi:10.1029/2007GL032904.

Lamarque, J.-F., and Coauthors, 2010: Historical (1850-2000) gridded anthropogenic and biomass burning emissions of reactive gases and aerosols: Methodology and application. *Atmos. Chem. Phys.,* **10,** 7017–7039, doi:10.5194/acp-10-7017-2010.

——, G. P. Kyle, M. Meinshausen, K. Riahi, S. J. Smith, D. P. van Vuuren, A. Conley, and F. Vitt, 2011: Global and regional evolution of short-lived radiatively-active gases and aerosols in the Representative Concentration Pathways. *Climatic Change,* **109,** 191–212, doi:10.1007/s10584-011-0155-0.

Landrum, L., M. M. Holland, D. P. Schneider, and E. Hunke, 2012: Antarctic sea ice climatology, variability and late twentieth-century change in CCSM4. *J. Climate,* in press.

Lawrence, P. J., and Coauthors, 2012: Simulating the biogeochemical and biogeophysical impacts of transient land cover change and wood harvest in the Community Climate System Model (CCSM4) from 1850 to 2100. *J. Climate,* **25,** 3071–3095.

Lean, J., 2000: Evolution of the sun's spectral irradiance since the maunder minimum. *Geophys. Res. Lett.,* **27,** 2425–2428.

Levitus, S., J. I. Antonov, T. P. Boyer, R. A. Locarnini, H. E. Garcia, and A. V. Mishonov, 2009: Global ocean heat content 1955-2008 in light of recently revealed instrumentation problems. *Geophys. Res. Lett.,* **36,** L07608, doi:10.1029/2008GL037155.

Lumpkin, R., and K. Speer, 2007: Global ocean meridional overturning. *J. Phys. Oceanogr.,* **37,** 2550–2562.

Meehl, G. A., and C. Tebaldi, 2004: More intense, more frequent and longer lasting heat waves in the 21st century. *Science,* **305,** 994–997.

——, W. M. Washington, C. Amman, J. M. Arblaster, T. M. L. Wigley, and C. Tebaldi, 2004: Combinations of natural and anthropogenic forcings and twentieth century climate. *J. Climate,* **17,** 3721–3727.

——, ——, W. D. Collins, J. M. Arblaster, A. Hu, L. E. Buja, W. G. Strand, and H. Teng, 2005: How much more global warming and sea level rise? *Science,* **307,** 1769–1772.

——, and Coauthors, 2006: Climate change projections for twenty-first century and climate change commitment in the CCSM3. *J. Climate,* **19,** 2597–2616.

——, and Coauthors, 2007: Global climate projections. *Climate Change 2007: The Physical Science Basis,* S. Solomon et al., Eds., Cambridge University Press, 747–845.

——, J. M. Arblaster, and W. D. Collins, 2008: Effects of black carbon aerosols on the Indian monsoon. *J. Climate,* **21,** 2869–2882.

——, and Coauthors, 2012: Relative outcomes of climate change mitigation related to temperature versus sea level rise. *Nat. Climate Change,* in press.

Meinshausen M., N. Meinshausen, W. Hare, S. C. B. Raper, K. Frieler, R. Knutti, D. J. Frame, and M. R. Allen, 2009: Greenhouse emission targets for limiting global warming to 2°C. *Nature,* **458,** 1158–1163.

Moss, R., and Coauthors, 2010: The next generation of scenarios for climate change research and assessment. *Nature,* **463,** 747–756, doi:10.1038/nature08823.

Murphy, D. M., and Coauthors, 2009: An observationally based energy balance for the Earth since 1950. *J. Geophys. Res.,* **114,** D17107, doi:10.1029/2009JD012105.

Peacock, S., 2012: Projected twenty-first century changes in temperature, precipitation and snow cover over North America in CCSM4. *J. Climate,* in press.

Stott, P. A., and C. E. Forest, 2007: Ensemble climate predictions using climate models and observational constraints. *Philos. Trans. Roy. Soc.,* **A365,** 2029–2052.

Taylor, K. E., R. J. Stouffer, and G. A. Meehl, cited 2009: A summary of the CMIP5 experimental design. [Available online at http://www-pcmdi.llnl.gov/.]

——, ——, and ——, 2012: An overview of CMIP5 and the experiment design. *Bull. Amer. Meteor. Soc.,* **93,** 485–498.

Tebaldi, C., J. M. Arblaster, K. Hayhoe, and G. A. Meehl, 2006: Going to the extremes: An intercomparison of model-simulated historical and future changes in extreme events. *Climatic Change,* **79,** 185–211, doi:10.1007/s10584-006-9051-4.

Teng, H., W. M. Washington, G. Branstator, G. A. Meehl and J.-F. Lamarque, 2012: Potential impacts of Asian carbon aerosols on future U.S. warming. *Geophys. Res. Lett.,* in press.

Trenberth, K., J. Berry and L. Buja, 1993: Vertical interpolation and truncation of model-coordinate data. NCAR Tech. Rep. NCAR/TN-396, 54 pp.

van Vuuren, D. P., and Coauthors, 2011: The representative concentration pathways: An overview. *Climatic Change,* **109,** 5–31, doi:10.1007/s10584-011-0148-z.

Vavrus, S., and Coauthors, 2012: Twenty-first-century Arctic climate change in CCSM4. *J. Climate,* **25,** 2696–2710.

Wang, Y.-M., J. L. Lean, and N. R. Sheeley Jr., 2005: Modeling the Sun's magnetic field and irradiance since 1713. *Astrophys. J.,* **625,** 522–538.

Washington, W. M., and Coauthors, 2000: Parallel climate model (PCM) control and transient simulations. *Climate Dyn.,* **16,** 755–774.